TECHNICAL MEMORANDUM

813

Shallow-water version of the Freak Wave Warning System

Peter A.E.M. Janssen

Research Department

November 2017

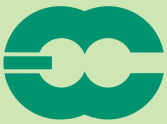

European Centre for Medium-Range Weather Forecasts
Europäisches Zentrum für mittelfristige Wettervorhersage
Centre européen pour les prévisions météorologiques à moyen terme

Series: ECMWF Technical Memoranda

A full list of ECMWF Publications can be found on our web site under:
http://www.ecmwf.int/en/research/publications

Contact: library@ecmwf.int

European Centre for Medium-Range Weather Forecasts
Shinfield Park, Reading, RG2 9AX, England

Abstract

The ECMWF freak wave warning system is based on a random time series analysis using the envelope wave height. The key quantity of interest is the maximum envelope wave height distribution which for (weakly) nonlinear systems depends on envelope skewness and kurtosis. Expressions for skewness and kurtosis for general spectra are presented, but they are very cumbersome. Therefore, a simple parametrization of skewness and kurtosis of the bound waves and the contribution of the free waves to kurtosis is presented. These parametrisations are validated against computations using the theoretical expressions of the statistical parameters. By adjusting some free parameters in the parametrizations a good agreement with the 'exact' computations is found. It is suggested to use these parametrizations in the operational version of ECMWF's freak wave warning system.

1 Introduction.

In the past 15 years there has been considerable progress in our understanding of the occurrence of freak waves. The notion of freak waves was first introduced by Draper (1965). In the early days, these extreme sea states were discussed in the context of linear wave theory for which the corresponding probability density function is the Rayleigh distribution (Dean, 1990), and extreme events were very unlikely. For example, the probability that an individual wave has an envelope wave height which is three times the mean wave height turns out to be about 2×10^{-9}. Recently it was established that nonlinear effects related to the presence of bound waves and non-resonant four wave interactions have a profound impact on the statistics of extreme events. Following the approach of Janssen (2015b) these nonlinear effects increase the probability of extremes by a factor of 100.

Another important advance is related to developments started by J. Adler (1981) who studied the extreme value problem in space and time. So far researchers have concentrated on the estimation of the probability of extremes from a time series at a certain point in space. From a modeling point of view it should be realized, however, that it is not really possible to give sea state or probability estimates at one location. Wave forecasting is based on a statistical representation of the sea state in terms of the wave spectrum. Here, the wave spectrum gives an ensemble averaged description of the sea state in a domain of the size of the $L_x \times L_y$ km^2 surrounding the location of interest (Nowadays, global operational wave forecasting models have a typical spatial resolution of about 15 km.). Likewise, one may obtain an ensemble averaged probability distribution function for quantities such as the envelope wave height or (linear) wave energy. To be more specific, it is possible to determine the probability that in a chosen domain parameters such as envelope wave height or wave energy exceed a chosen value, and in order to achieve this we need to obtain the maximum envelope wave height p.d.f. (which will be given in this note) and we need an estimate of the number of events in a spatial domain of a given size. Following the work of Adler (1981), which is based on insights from topology, the number of extreme events is larger than could be expected from a simple argument using the decorrelation scales in the spatial domain. Combining the two developments, namely, introduction of nonlinear effects and estimation of the number of extreme events, it turns out that extreme events such as the famous Draupner wave and the Andrea wave are much more likely than the early expectations in the 1960's and 1970's. (Cavaleri *et al.* (2016), Fedele (2012), Benetazzo *et al.* (2015), Janssen (2015b)).

In this note, I am going to describe the work that has been done to convert the theoretical approach to estimate extreme events into a practical application which can be used in the ECMWF freak wave warning system. In §2 a brief overview of the method is given. Starting point for this is Janssen (2014) which develops an analysis of time series based on the envelope ρ. The square of the envelope is a measure for the potential energy of the waves. In fact, the total energy $E = \rho^2/2$. This is a popular

measure in fields such as nonlinear optics because only the envelope of the wave train can be measured but not the wave itself. Here, I suggest to use the same measure in the field of ocean waves as it is a measure that has physical relevance. For convenience, and to stay close to oceanographic practice, the envelope waveheight h is introduced which is defined to be twice the envelope height, i.e., $h = 2\rho$. If the effects of nonlinearity are small, the p.d.f. of envelope wave height may be obtained by means of a Taylor expansion of the logarithm of its generating function. This basically gives an expansion around the Rayleigh distribution where the relevant expansion coefficients are the third-order (skewness) and fourth-order (excess kurtosis) cumulants of the random envelope. Following this approach, envelope skewness and excess kurtosis for the bound waves can be obtained from the wave spectrum following a procedure described in Janssen (2009), who applied it to obtain the surface elevations statistics, while the contribution from the free waves is obtained from Janssen (2003) and Mori and Janssen (2006).

This approach seems to work well as follows from comparisons with p.d.f.'s observed in the laboratory. Nevertheless, this statistical theory has a restricted range of validity. This follows from a comparison with maximum wave height data obtained in the field by Janssen and Bidlot (2009) (see their Fig. 8) where it is evident that the theoretical p.d.f. starts to deviate from the observed one for extreme sea states with $h_{max}/H_S > 2.5$. Since extreme events, such as the Draupner wave, have a maximum envelope wave height that is about three times the significant wave height, it follows that this event is clearly outside the range of validity of the nonlinear approach and an extension of the domain of validity is required. Nowadays there is evidence that for very extreme states the p.d.f. has an exponential tail. Particularly convincing evidence is found from experimental work in nonlinear optics and liquid crystals. The work of Montina *et al.* (2009) suggests that the statistics of the fluctuations can be approximated by a simple empirical form, a stretched exponential distribution. Using this distribution to model the tail of the p.d.f., Janssen (2015b) has shown that this results in a satisfactory agreement with Monte Carlo simulations of a random weakly nonlinear Stokes wave down to values of the simulated p.d.f. of order 10^{-7}.

Given the form of the p.d.f. of envelope wave height, the next step is to establish the maximum envelope wave height probability distribution. In the present ECMWF Freak Wave Warning system, Goda's maximum wave height distribution has been used. In Goda's approach an important parameter is the number of events, of which a choice needs to be made which introduces some arbitrariness. An alternative has been suggested by Naess (1982). His method is based on the reasonable assumption that for envelope time series the number of level upcrossings by the envelope $\rho(t)$ is asymptotically Poisson distributed when the level height increases. In Janssen (2015a) it has been shown that, in particular for the tail of the maximum wave height distribution, Naess's idea yields for linear waves a very good agreement with Monte Carlo simulations of the p.d.f. of maximum envelope wave height. Therefore, it was decided to use the Naess approach in the operational implementation.

Finally, I present work that is required to develop an operationally feasible warning system. It should be realized that the expression for skewness and kurtosis introduced by Janssen (2003) and Janssen (2009) involve the evaluation of four and six dimensional integrals which would result in far too long operational run times. For this reason, I am going to introduce simple parametrizations of envelope skewness and kurtosis, which are based on results obtained from the narrow-band version of the theoretical expression for skewness and kurtosis. These parametrizations are validated against exact computations of the relevant statistical parameters for the Draupner wave and the Andrea Storm, and a reasonable agreement is obtained.

2 The method.

Following Janssen (2014) a time series analysis based on the envelope wave height will be used. In this reference, it is shown that this method gives an accurate estimation of the joint p.d.f. of wave height and period for linear waves and that it is possible to extend the approach into the weakly nonlinear regime. To make things more quantitative let us introduce the local energy $\mathscr{E} = \langle \eta^2 \rangle$ and introduce the envelope ρ according to $\eta = \rho \cos\theta$. One finds

$$\mathscr{E} = \frac{1}{2}\rho^2, \tag{1}$$

while the normalized local energy is given by $E = \mathscr{E}/\sigma^2$ with $\sigma^2 = m_0$ the variance of the sea surface elevation and m_0 the zeroth moment of the spectrum. The value $E = 1$ then corresponds to a local wave energy which equals the average wave energy in the domain of interest. Events such as the Draupner wave event and the Andrea storm have $E \simeq 20$ which illustrates that at the focal point there was a considerable amplication of wave energy, therefore these events are quite extreme. As an alternative measure I introduce the local wave height as twice the envelope height ρ and the normalized envelope wave height h becomes

$$h = \frac{2\rho}{4\sigma} \tag{2}$$

and the relation between normalized envelope wave height and local energy is $E = 2h^2$ so that for the Draupner event $h_{max} = 3.1$, while for the Andrea event $h_{max} = 3.26$.

2.1 Statistics in the weakly nonlinear regime.

Janssen (2014) has obtained the following envelope wave height distribution for a weakly nonlinear sea state. It reads

$$p(h) = 4he^{-2h^2}\left\{1 + C_4\left(2h^4 - 4h^2 + 1\right) + C_3^2\left(4h^6 - 18h^4 + 18h^2 - 3\right)\right\}. \tag{3}$$

where the parameters C_4 and C_3^2 are obtained from knowledge of the two-dimensional wave spectrum and are related to the kurtosis and skewness of the sea state. Here

$$C_4 = \frac{\kappa_4}{8}, \tag{4}$$

and the envelope kurtosis κ_4 is given by

$$\kappa_4 = \kappa_{40} + 2\kappa_{22} + \kappa_{04} \tag{5}$$

while

$$C_3^2 = \frac{\kappa_3^2}{72},\ \kappa_3^2 = 5(k_{30}^2 + \kappa_{03}^2) + 9(\kappa_{21}^2 + \kappa_{12}^2) + 6(\kappa_{30}\kappa_{12} + \kappa_{03}\kappa_{21}) \tag{6}$$

The κ's refer to a number of cumulants of the joint distribution of the surface elevation $\eta = \rho\cos\theta$ and its Hilbert transform $\zeta = \rho\sin\theta$. In addition, it is noted that both free and bound waves may contribute to the cumulants. The general expressions for skewness and kurtosis parameters are given in Appendix A, which also provides explicit expressions for the case of a narrow-band wave train.

From the pdf for wave height, Eq. (3), one may then immediately obtain the pdf of wave energy, since $p(h)\mathrm{d}h = p(E)\mathrm{d}E$ with $E = 2h^2$. The result is

$$p(E) = e^{-E}\left[1 + C_4 A(E) + C_3^2 B(E)\right], \tag{7}$$

where

$$A(E) = \frac{1}{2}E^2 - 2E + 1,\ B(E) = \frac{1}{2}E^3 - \frac{9}{2}E^2 + 9E - 3. \tag{8}$$

Finally, for the purpose of estimating the maximum wave height distribution the exceedance probability $P(E > E_c)$ is required. It follows from an integration of the pdf (7) from E to infinity, with the result

$$P(E) = e^{-E}\left[1 + C_4 A(E) + C_3^2 B(E)\right], \tag{9}$$

where

$$A(E) = \frac{1}{2}E(E-2),\ B(E) = \frac{1}{2}E(E^2 - 6E + 6). \tag{10}$$

It should be realized, however, that the expressions for the p.d.f. and c.d.f. have only a restricted range of validity. For example, for given stats for skewness and kurtosis the p.d.f. (3) underestimates the true p.d.f. for large envelope wave heights in the range $h > 2.5$. In other words, the theoretical approach fails just in the wave height range where a number of extreme events, such as the Draupner wave and the Andrea storm, have been reported. The range of validity of the theoretical approach therefore needs to be extended.

2.2 Behaviour of the tail of the p.d.f.

Nowadays there is ample evidence that for very extreme (sea) states the pdf of envelope wave height has an exponential tail, resulting, compared to the present theory, in much larger probabilities for extreme events. Evidence for an exponential tail follows from numerical simulations (e.g. Montina *et al.* (2009), Walczak *et al.* (2015), Janssen (2014), Janssen (2015b)), and comparison with field data (Janssen and Bidlot, 2009). Also, in nonlinear optics and liquid crystals a considerable amount of experimental evidence is available that suggests that this tail is exponential. It is therefore important to modify the present approach by adding an exponential tail. For extreme waves in a nonlinear optical cavity Montina *et al.* (2009) have noted that the observed probability distribution function for intensity E can be well approximated by a stretched exponential form, involving a number of fitting parameters. Following this idea, it was realized, after some trial and error, that by using a stretched exponential to approximate the cumulative distribution function only one fitting coefficient was needed. The general form used to extend the range of validity of the theoretical c.d.f. (9) for normalised wave energy reads

$$P(E) = \int_E^\infty \mathrm{d}x\, p(x) = e^{-z},\ z = -\alpha + \sqrt{\alpha^2 + \beta E}, \tag{11}$$

where (see Janssen (2015b)) $\beta = 2(\alpha + 1)$ as for zero energy the c.d.f. should equal 1, so that for matching purposes one only needs to determine the parameter α. The origin of (11) is not well understood by the present author. However, it should be pointed out that the most simple nonlinear system that has a similar c.d.f for wave energy is one that only has a first and bound, second harmonic (Janssen, 2017).

This simple form has some interesting properties. First of all, the condition $P(E=0)=1$ is automatically satisfied so that the underlying pdf $p(E)$ is normalized to 1. Second, for small E Taylor expansion of z gives $z=\beta E/(2\alpha)$ hence

$$\lim_{E\to 0} P(E) = e^{-\frac{\beta}{2\alpha}E}, \tag{12}$$

while for large E one finds

$$\lim_{E\to \infty} P(E) = e^{-\sqrt{\beta E}}. \tag{13}$$

Realizing that $E=2h^2$ this means that in terms of envelope wave height we have for small E a Gaussian distribution while for large E the distribution is exponential.

By differentiation of the c.d.f. (11) it is straightforward to obtain the pdf $p(E)$. By definition

$$p(E) = -\frac{\partial P}{\partial E}$$

so that

$$p(E) = \frac{\beta}{2(z+\alpha)} e^{-z},\ z = -\alpha + \sqrt{\alpha^2+\beta E}.$$

It is then straightforward to obtain the envelope wave height p.d.f. from the condition $p(h)\mathrm{d}h = p(E)\mathrm{d}E$ and the result is

$$p(h) = \frac{2\beta h}{(z+\alpha)} e^{-z}. \tag{14}$$

In a moment it will be seen that this form of the envelope wave height p.d.f. is an adequate approximation for both the weakly nonlinear regime and for the tail of the distribution.

A relation for α is now obtained by matching the empirical c.d.f. (11) with the theoretical one, given in Eq. (9), which is denoted by P_{th}. The fitting constant α then follows from the condition that at the edge of the range of validity, taken as $E_b = 10$ (corresponding to $h=2.2$), the empirical CDF equals the theoretical one, i.e. $P(E_b) = P_{th}(E_b)$. This gives for α,

$$\alpha = \frac{f_b^2 - 2E_b}{2(E_b+f_b)},\ f_b = \log P_{th}(E_b). \tag{15}$$

where f_b is the logarithm of the theoretical c.d.f. at the boundary given by $E=E_b$. In this manner a connection between skewness and kurtosis of the sea state, via f_b, and the fitting parameters of the empirical CDF has been established. For relatively small values of C_4 and C_3 this matching procedure works well, as reported in Janssen (2015b).

It is important to check the validity of the statistical distribution presented in this note by means of a Monte Carlo simulation, and this subject has been more extensively discussed in Janssen (2015b). Since the interest is in extreme events with probabilities of the order 10^{-6} the number of ensemble members N_{ens} needs to be quite large. By trial and error, I have taken $N_{ens} = 50,000,000$, in order to obtain smooth results for the pdf. Assuming that the envelope waveheight pdf is determined by the skewness factor C_3 and the kurtosis factor C_4 only, one may use any nonlinear system in the numerical simulation as long as it has the same statistical parameters. For this reason a Monte Carlo simulation is performed with a Stokes wave train, where the amplitude a is drawn from a Rayleigh distribution while the random

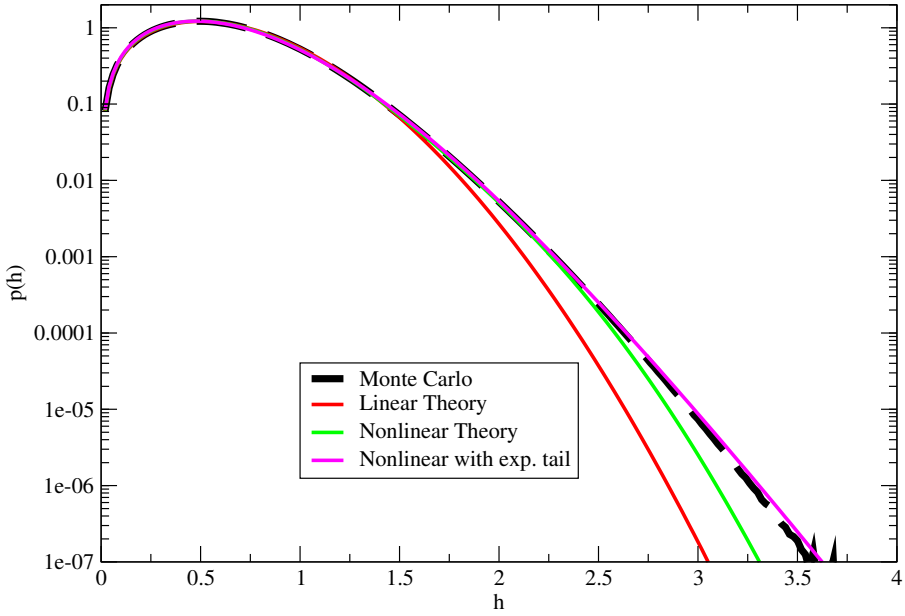

Figure 1: Probability distribution function of envelope wave height for a significant steepness of 0.06 and a dimensionless depth of 1.45, mimicking the Draupner wave event. The Monte Carlo simulation shows clear evidence that the tail of the distribution is exponential. Nonlinear theory combined with the stretched exponential of Residori is in good agreement with the simulation.

phase is drawn from a uniform distribution. We have studied the properties of the envelope waveheight of this nonlinear system. The envelope waveheight pdf, as obtained from the Monte Carlo Simulation, is shown in Fig. 1. Over a wide range of values, between 10^{-6} and 10^{-2}, the logarithm of the pdf behaves as a straight line, hence the pdf follows an exponential law. For comparison, also shown are results according to linear theory, and it is clear that this gives a large underestimation of the frequency of extreme events. The nonlinear theory discussed by Janssen (2014) shows good agreement with the simulation up to a waveheight of $h = 2.5$, but the probability of extreme events such as the Draupner case with $h = 3.1$ is considerably underestimated. The approach that adds, using the method detailed here, an exponential tail is found to agree very well with the numerical simulation. In fact, the violet line, labeled Nonlinear with exp. tail, corresponds to Eq. (14), therefore the stretched exponential captures both the weakly nonlinear regime with $h < 2.5$ and the tail region with $h > 2.5$. From now onwards I will use the stretched exponential form for describing the statistical distribution for extreme events.

2.3 Maximum envelope wave height distribution:linear theory.

In order to derive the p.d.f. of maximum envelope wave height we need information on the statistics of the envelope wave height time series and we need the length T_L of the time series. The relevant statistics are the envelope wave height distribution $p(h)$, the cumulative wave height distribution (or the

cumulative distribution function, cdf)

$$P(h) = \int_h^\infty \mathrm{d}h\, p(h),$$

and the joint pdf of envelope wave height h and its time derivative $\dot{h}$. Here, we concentrate on linear theory firstly and in the next sub section we sketch how to extend results for weakly nonlinear theory. As according to linear theory the envelope wave height distribution is given by the Rayleigh distribution (see Eq. (3)),

$$p(h) = 4he^{-2h^2}, \tag{16}$$

the cumulative distribution function becomes

$$P(h) = e^{-2h^2}. \tag{17}$$

Again assuming linear waves, the joint probability distribution (j.p.d.) of envelope wave height h and its time derivative $\dot{h}$ is given by

$$p(h,\dot{h})) = \frac{8h}{\sqrt{2\pi}} e^{-2(h^2+\dot{h}^2)}, \tag{18}$$

where $\dot{h}$ has been normalized by means of the parameter $m_0^{1/2}\nu\bar{\omega}$ with $\bar{\omega} = m_1/m_0$ the mean angular frequency while $\nu = (m_0 m_2/m_1^2 - 1)^{1/2}$ is the width of the frequency spectrum. Note that by considering the j.p.d. of h and $\dot{h}$ the frequency scale $\nu\bar{\omega}$ is introduced in a natural way which corresponds to the inverse of the relevant timescale of the wave groups. As time has been made dimensionless with this frequency scale the length T_l of the timeseries has to be scaled accordingly, hence the dimensionless length is $T_L^* = T_L \times \nu\bar{\omega}$. The result (18) is valid for a Gaussian sea state and can be obtained in a straightforward manner from the well-known expression of the j.p.d. of envelope ρ and phase ϕ and its time derivatives (see e.g. Janssen (2014)). Integration over phase ϕ and its derivative $\dot{\phi}$ and introduction of the envelope wave height which is twice the envelope then results in (18). Alternatively, one may argue that h and $\dot{h}$ are independent and that the joint pdf of h and $\dot{h}$ is simply the product of the marginal distributions of h and $\dot{h}$, i.e. the product of a Rayleigh distribution for h and a Gaussian distribution for $\dot{h}$.

In the present ECMWF Freak Wave Warning system Goda's maximum wave height distribution has been used. In Goda's approach an important parameter is the number of events N, which has to be chosen and therefore introduces some arbitrariness. As already discussed by Janssen (2015a), in Goda's approach the maximum wave height distribution is obtained by writing down the probability that for given number of (independent) events N the maximum envelope height has a certain chosen value. In other words, the maximum wave height distribution $p_{max}(h_{max})$ is the probability that a certain event attains the maximum value multiplied by the probability that all other events are below the maximum value while realizing that there are N possibilities. In the continuum limit, i.e. for large N, the maximum wave height distribution assumes, with $\mathscr{G}(h) = -NP(h)$, the simple form

$$p_{max}(h = h_{max}) = \frac{\mathrm{d}\mathscr{G}}{\mathrm{d}h} \exp(\mathscr{G}) = Np(h_{max}) \exp[-NP(h_{max})], \tag{19}$$

where $p(h)$ is the p.d.f. of envelope wave height and $P(h)$ is the exceedance probability. Then, the probability that maximum envelope wave height is larger than a given value, say h_c, becomes for large N,

$$P(h_{max} > h_c) \simeq 1 - \exp(\mathscr{G}(h_c)) = 1 - \exp(-NP(h_c)).$$

For linear waves the statistics are Gaussian and the exceedance probability is given in (17) resulting in the well-known double exponential law

$$P(h_{max} > h_c) = 1 - \exp\{-Ne^{-2h_c^2}\}$$

for the maximum envelope wave height probability. Note that in Goda's method the number of events N is independent of the exceedance level h_c.

So the question now is how to choose the number of independent events. It is customary to define an event with respect to a chosen reference level h_c. An event is then a part of a time series of length T_L that starts where the envelope has an upcrossing at level h_c and that finishes at the next upcrossing. The frequency of events is then determined by the upcrossing frequency. The total number of events in a time series of length T_L then determines the number of degrees of freedom N. For a more complete discussion see Elgar *et al.* (1984), where it follows that N and also parameters such as the number of waves in a group depend on the chosen reference level, but it is not clear which level to choose. Therefore, in order to make Goda's method work, which relies on a constant number of degrees of freedom, it may be appropriate to introduce an average upcrossing frequency. The first measure of frequency that came to mind is basically the average of the rate of change of h with time, $\dot{h}$ normalized with h itself. Hence, the average frequency of events, determined by the average upcrossing frequency, becomes

$$\langle f_{up} \rangle = \langle \dot{h}/h \rangle = \int_0^\infty \mathrm{d}h \int_0^\infty \mathrm{d}\dot{h}\; p(h,\dot{h})\; \dot{h}/h$$

where $p(h,\dot{h})$ is the joint p.d.f. of h and $\dot{h}$. Making use of the joint pdf of h and $\dot{h}$ in Eq. (18) and performing the integrations one immediately finds the simple result

$$\langle f_{up} \rangle = 1$$

and the average number of events becomes

$$N = \langle f_{up} \rangle T_L^* = \nu \bar{\omega} T_L.$$

This result reflects that the number of degrees of freedom is determined by the number of wave groups. It is emphasized that I have only made plausible how N depends on the relevant parameters. To some extent the result is uncertain because I have made the choice to connect the number of events with the average upcrossing frequency.

An alternative method to obtain the maximum envelope wave height distribution has been suggested by Naess (1982). His approach is based on the reasonable assumption that for envelope time series the number of level upcrossings by the envelope $\rho(t)$ is asymptotically Poisson distributed when the level height increases. In Janssen (2015a) it has been shown that, in particular for the tail of the maximum wave height distribution, Naess's idea results for linear waves in very good agreement with Monte Carlo simulations of the p.d.f. of maximum envelope wave height.

Naess (1982) states, based on Cramér's theorem, that if $\eta(t)$ is a stationary Gaussian process, satisfying certain mild restrictions, then the number of level upcrossings by $\eta(t)$ is asymptotically Poisson distributed when the level height increases. Naess assumes that this then also holds for the associated envelope process. Let f_{up} be the mean frequency of upcrossings of the level h_c, then for a Poisson process

$$P = \mathrm{Prob}\{h \le h_c; 0 \le t \le T_L^*\} = e^{-f_{up} T_L^*}.$$

The average frequency with wich $h(t)$ crosses a reference level h_c with a positive slope, hence positive $\dot{h}$, is then given by

$$f_{up} = \int_0^\infty \mathrm{d}\dot{h}\; \dot{h} p(h_c, \dot{h}),$$

and substitution of (18) and carrying out the integration gives

$$f_{up} = \frac{2h_c}{\sqrt{2\pi}} e^{-2h_c^2}.$$

We now fix T_L^* and denote by $H = \max(h)$ for time $t \in (0, T_L^*)$. Using this in the cdf P one finds

$$P_H(h) = \exp\{-hN_{slc}e^{-2h^2}\}, \tag{20}$$

where P_H denotes the probability distribution function of maximum wave height H, and,

$$N_{slc} = 2T_L^*/\sqrt{2\pi} \tag{21}$$

is the number of (up)crossings at the significant level $h = 1$ (Here, the subscript 'slc' stands for significant level crossings). The maximum envelope height distribution then follows from $p_{max}(h) = dP_H/dh$, or,

$$p_{max} = (4h^2 - 1)\, N_{slc}\, e^{-2h^2} P_H(h), \quad \text{where } h \geq \frac{1}{2}. \tag{22}$$

The restriction $h \geq \frac{1}{2}$ is added in order to prevent the pdf from becoming negative. In addition, note that the approach by Naess is only valid for large level crossings, presumably because for large levels the level upcrossings are statistically independent since these are rare events. An important point to make is that in the present result the dependence of the average number of wave groups N on the reference level has been taken into account, while in the result (19) N has been assumed a constant. As a consequence, the large h behaviour of (22) differs from (19) because it involves an additional factor h. This different asymptotic

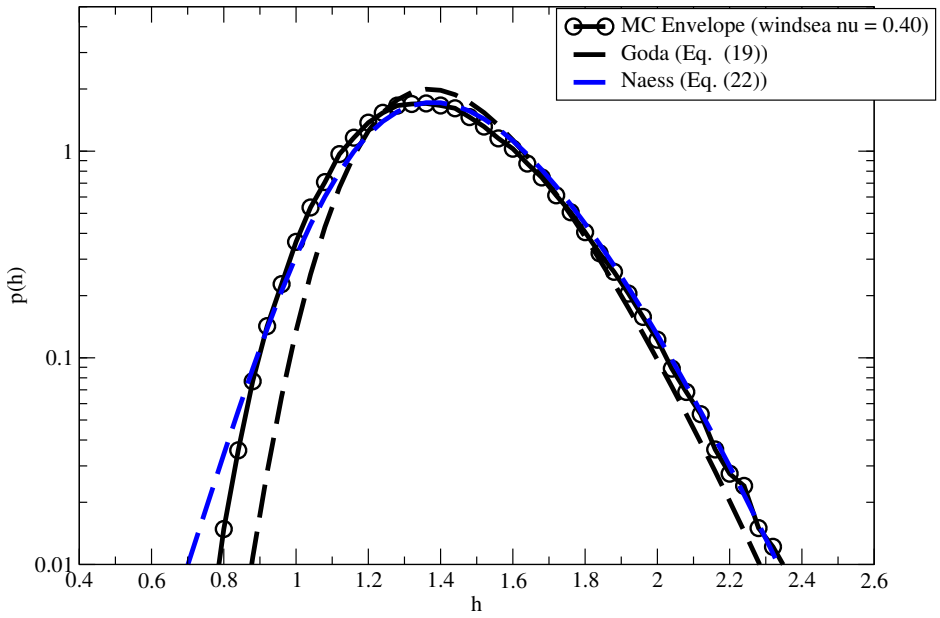

Figure 2: The pdf of maximum envelope wave height for 'old' wind sea ($\gamma = 1$). The duration of the time series is 10 wave periods. Shown is the comparison between results from Monte Carlo simulations, and the theoretical result from Eq. (19) and Naess' (1982) Eq. (22). In the Monte Carlo simulations both amplitude and phase of the waves are regarded as stochastic variables.

behaviour of the two results for maximum wave height distribution is born out by a comparison of (22) and (19) with Monte Carlo simulations of the sea state with a Pierson-Moskovitz spectrum, as shown in Fig. 2. Here, it is important to point out that a Monte Carlo simulation was performed where amplitudes are drawn randomly from a Rayleigh distribution while phases were drawn from a uniform distribution. Fig. 2 shows clearly that the Naess expression for the maximum envelope waveheight distribution is in better agreement with the Monte Carlo result, in particular for the tails of the distribution.

2.4 Maximum envelope wave height: nonlinear extension and expectation value.

In the previous sections we have found that for linear waves Naess' expression is adequate in describing the maximum envelope wave height distribution. The extension towards nonlinear waves is not trivial, however, because it requires deriving the joint probability distribution of h and $\dot{h}$ in the weakly nonlinear case. In principle this can be done but it is simply a matter of a lot of work. Therefore, at the moment I can only make an educated guess of the form of a maximum envelope wave height p.d.f., based, of course, on the findings thus far.

I will do the following discussion both in terms of the wave energy $E = 2h^2$, and in terms of the envelope wave height h. Based on Eq. (20) I posit that the maximum envelope wave height distribution has the form

$$p_{max}(h) = \frac{\mathrm{d}\mathscr{G}}{\mathrm{d}h} \exp(\mathscr{G}), \tag{23}$$

where $\mathscr{G}$ involves the stretched exponential

$$\mathscr{G} = -N \exp(-z),\ z = -\alpha + \sqrt{\alpha^2 + \beta E}. \tag{24}$$

and, in keeping with Naess' approach, the number of degrees of freedom depends on the reference level, i.e.

$$N = N_{slc} \left(\frac{E}{2} \right)^{1/2} \tag{25}$$

where N_{slc} is given by (21). Finally, the parameters α and β follow, see Eqns. (11-15), from matching the stretched exponential distribution with the weakly nonlinear c.d.f. of (9) so that the fitting parameters depend on skewness and kurtosis of the envelope time series.

An important quantity to measure the extremity of an event is the exceedance probability that energy or wave height is larger than a critical value. Using (23) one finds

$$P(h > h_c) = \int_{h_c}^{\infty} \mathrm{d}h\ p_{max}(h) = 1 - \exp(\mathscr{G}). \tag{26}$$

This quantity is very sensitive to the tail of the maximum envelope wave height distribution, but it gives important information on, for example, the probability that waves hit the lower deck of an oil rig.

A more robust indicator of extreme events is the expectation value of maximum envelope wave height. It is here defined using the expectation value of maximum wave energy $\langle E_{max} \rangle$, defined as

$$\langle E_{max} \rangle = \int_0^{\infty} \mathrm{d}E\ E\ p_{max}(E), \tag{27}$$

with

$$p_{max}(E) = \frac{\mathrm{d}\mathscr{G}}{\mathrm{dE}} \exp \mathscr{G}. \tag{28}$$

Then, maximum wave height is defined as

$$\langle H_{max} \rangle = \sqrt{\frac{1}{2} \langle E_{max} \rangle}, \tag{29}$$

as $E = 2h^2$.

Now it should be realized that the maximum energy distribution $p_{max}(E)$ is a very narrow distribution. For example the dependence of the number of degrees of freedom $N(E)$ on energy E is fairly weak compared to the stretched exponential function $\exp(-z)$. As a consequence, the function $N(E)$ of (25) may be approximated by $N(\langle E\rangle)$ and is regarded as a constant in the integration. In that event, for large N the integral may be evaluated almost exactly (with error of $\mathcal{O}(\exp -N)$) with the result

$$\langle E_{max}\rangle = \frac{1}{\beta}\left[G_2 - 2G_1\left(\alpha + \log N\right) + \log N\left(2\alpha + \log N\right)\right], \tag{30}$$

where $N = N_{slc}\sqrt{\langle E_{max}\rangle/2}$, hence Eq. (30) is an implicit relation for $\langle E_{max}\rangle$. The symbols G_n, $n = 1,2$ denote integrals involving exponentials and logarithms. These are related to the Gamma function $\Gamma(1+z)$ and its derivatives,

$$\Gamma(1+z) = \int_0^\infty t^z e^{-t}\mathrm{d}t = \int_0^\infty e^{z\log t} e^{-t}\mathrm{d}t,$$

and therefore

$$G_n = \left.\frac{\mathrm{d}^n}{\mathrm{d}z^n}\Gamma\right|_{z=0} = \int_0^\infty \log^n t\; e^{-t}\mathrm{d}t, n = 1,2,3,\ldots$$

It may be shown that $G_1 = \Gamma'(1) = -\gamma$, while $G_2 = \Gamma''(1) = \gamma^2 + \pi^2/6$.

Although (30) is an implicit equation for the expectation value of maximum wave energy, it is straightforward to solve it by iteration. In practice, this iteration scheme converges very quickly, only 5 iteration are needed at the most. This follows from a comparison with results from a numerical computation of the integral (27) where after 5 iterations agreement up to four digits was achieved.

Finally, it should be emphasized that the expression (30) is very elegant, and, compared to previous work (cf. Janssen, 2015a), it is much simpler. This is, of course, because of the use of the stretched exponential for the 'parent' distribution for envelope wave height. In addition, it should be noted that for a Gaussian sea state, which is achieved by taking the limit of $\alpha \to \infty$ (while realizing that $\beta = 2(\alpha+1)$) the expression for maximum wave energy simply becomes

$$\langle E_{max}\rangle = \gamma + \log N.$$

3 Parametrization of skewness and kurtosis.

In the present operational system parametrizations for skewness and kurtosis for free waves and bound waves are used in the estimation of probabilities for extreme events and for the expectation value of maximum envelope wave height. Strictly speaking, these parametrizations are only valid for the case of deep water. A shallow water parameterization is highly desirable because most off-shore operations take place in finite depth. We attempt to find these parametrizations by assuming, on the one hand, that the stats obtained from the general formulation for arbitrary spectra is the truth, while the approximate formulae for skewness and kurtosis are obtained by adjusting parameters in the corresponding narrow-band approximations in such a way that a reasonably good agreement with the truth is obtained.

Let us first discuss results for skewness and kurtosis using the general formulation for arbitrary spectra, which is then followed by a presentation of the simple parametrisations of the statistics of waves. Simulated WAM spectra were taken from two shallow water cases where freak wave events have been observed, namely the Draupner freak wave event from the 1^{rst} of January 1995, occurring at 15:20, and

the Andrea storm which occurred on midnight of the 9^{th} of November 2007. The Draupner event was hindcasted by Cavaleri *et al.* (2016) using the most recent version of the ECMWF coupled ocean-wave, weather forecasting system which has a resolution of 10 km in the horizontal and has 137 layers in the vertical. Just recently, L. Bertotti and L. Cavaleri have produced, in addition, a simulation for the Andrea storm with the same coupled system. In both cases the water depth at the location where the freak wave events occurred was 70 m and the dimensionless depth $k_p h$, with k_p the peak wave number and h depth, was during the extreme event in the intermediate depth regime as the range of dimensionless depth varies between 1.45 and 1.9.

The simulated spectra have, for an operational system, a fairly high resolution of 36 frequencies and 36 directions, where the frequencies are on a logarithmic grid and the directions are on a linear grid. In Fig. 3 a few examples of spectra are shown, one at the time of the Draupner event, one at the time of the Andrea freak wave and one example of a broad spectrum taken from the Andrea storm at noon on the 8^{th} of November 2007, illustrating that both narrow and broad-band spectra are present in the time series.

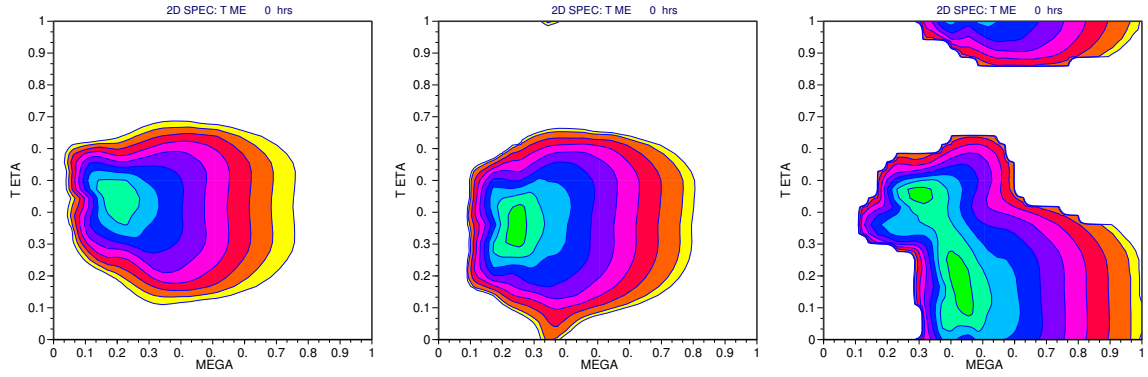

Figure 3: Left panel: Wave spectrum for Draupner event at 16:00 hrs on 1-1-1995; Middle panel: Andrea main event at midnight of 9-11-2007; Right panel: broad-band spectrum 12 hrs before the Andrea event.

An important point to note is that the wave spectra at the time of the extreme events have a more narrow directional distribution than a typical wind sea in deep water. In order to appreciate this point I show in

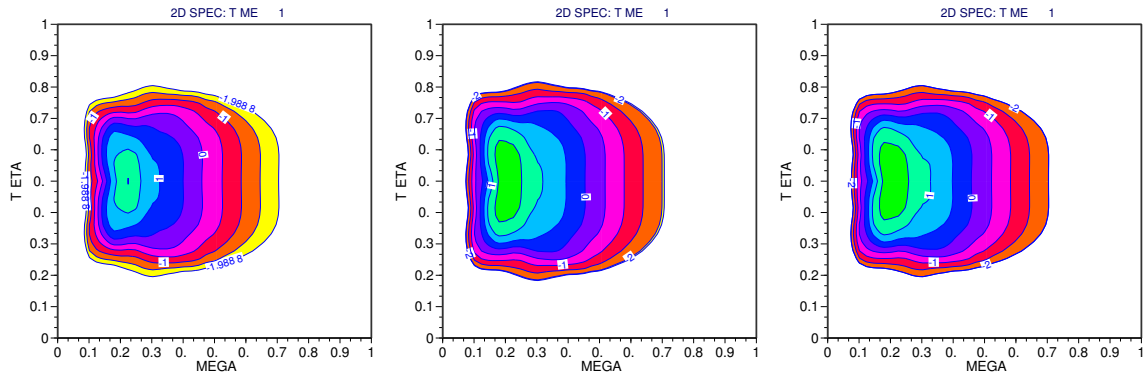

Figure 4: Left panel: Wave spectrum after one day wind forcing in shallow water; Middle panel: Wave spectrum after one day forcing in deep water; Right panel: Shallow water run with bottom friction switched off.

Fig. 4 the wave spectrum obtained from a one-gridpoint model run after 24 hours forcing with a wind speed of 18.45 m/s. In the left panel I show the result when depth h = 70 m, which corresponds to $k_p h = 1.9$, while the middle panel shows the result for deep water. Clearly, the deep water run gives a broader spectrum.

An interesting question to ask is which physical process is responsible for the narrowing of the directional spectrum in shallow water. In the context of a single gridpoint model it is fairly straightforward to investigate this issue. The first candidate is the wind input source function, but it turned out that the directional width of the growthrate by wind was very similar in deep and shallow water. The next candidate that was studied is the nonlinear transfer which contains a depth dependent amplification factor. Switching off the amplification factor did not result in an appreciable change of the width of the directional spectrum, however. Finally, it turned out, as shown in the right panel of Fig. 4, that switching off the bottom friction source function in the shallow water run explains to a large extent the reason why in shallow water the directional spectrum is narrower.

In order to quantify the differences I would like to introduce a robust measure of directional width near the peak of the spectrum. Usually, the directional width σ_θ is estimated using frequency dependent moments, i.e.

$$m_0 = \int \mathrm{d}\theta F(\omega,\theta),\; m_1 = \int \mathrm{d}\theta \cos(\theta-\overline{\theta})F(\omega,\theta),$$

with $\overline{\theta}$ the mean direction and $F(\omega,\theta)$ the two-dimensional wave spectrum. However, this is not such a robust measure and therefore I integrate the frequency dependent moments over a region around the angular peak frequency ω_p of width $2\Delta\omega$, i.e.

$$\overline{m}_0 = \int_{\omega_p-\Delta\omega}^{\omega_p+\Delta\omega} \mathrm{d}\omega \int \mathrm{d}\theta F(\omega,\theta),\; \overline{m}_1 = \int_{\omega_p-\Delta\omega}^{\omega_p+\Delta\omega} \mathrm{d}\omega \int \mathrm{d}\theta \cos(\theta-\overline{\theta})F(\omega,\theta), \tag{31}$$

and the measure of directional width becomes

$$\sigma_\theta = \sqrt{2(1-R_1)},\; R_1 = \overline{m}_1/\overline{m}_0 \tag{32}$$

The above definition of directional width will also be used in a simple parametrisation of dynamic kurtosis. Using the measure in (32) it is found that for the Draupner spectrum in Fig. 3 $\sigma_\theta = 0.32$ while for the deep-water case of Fig. 4 $\sigma_\theta = 0.55$, so there is a considerable difference in width. This difference is quite important for the estimation of the value of the dynamic kurtosis, as it depends on the square of directional width.

3.1 Results for skewness and kurtosis from exact computations.

Using the exact expressions given in the Appendix, i.e. (A7), (A22) and (A25), time series for skewness and kurtosis have been obtained from the simulated spectra for the Draupner and Andrea case. They are displayed in Fig. 5.

Noting that the Draupner freak wave occurred at 16:00 hrs while the Andrea event occured at 24 hrs, there is a striking difference between the two cases. During the Andrea event there is a clear sign that skewness and kurtosis have a maximum at the time of the freak wave event whereas for the Draupner wave this is only marginally evident for the skewness. In particular, the time series for kurtosis is fairly featureless.

Realizing that kurtosis consists of a dynamic part and a bound-wave part it is therefore also of interest to study their respective timeseries. They are displayed in Fig. 6.

The Figure shows that for both the Draupner event and the Andrea wave the bound-wave part of kurtosis reached an extremum at the time of the occurrence of the freak wave, while the dynamic part of the

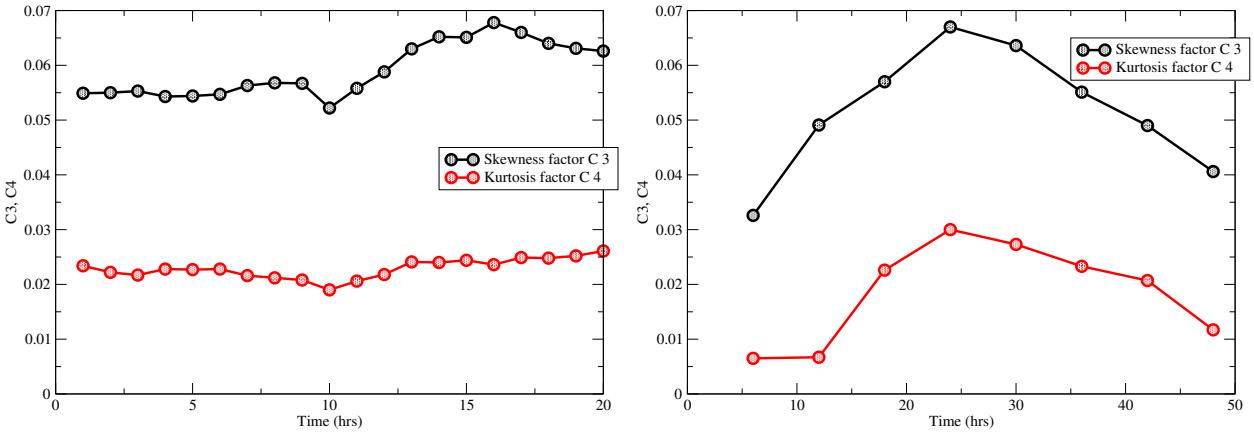

Figure 5: Evolution in time of skewness factor C_3 and kurtosis factor C_4 for the Draupner case (left panel) and the Andrea storm (right panel).

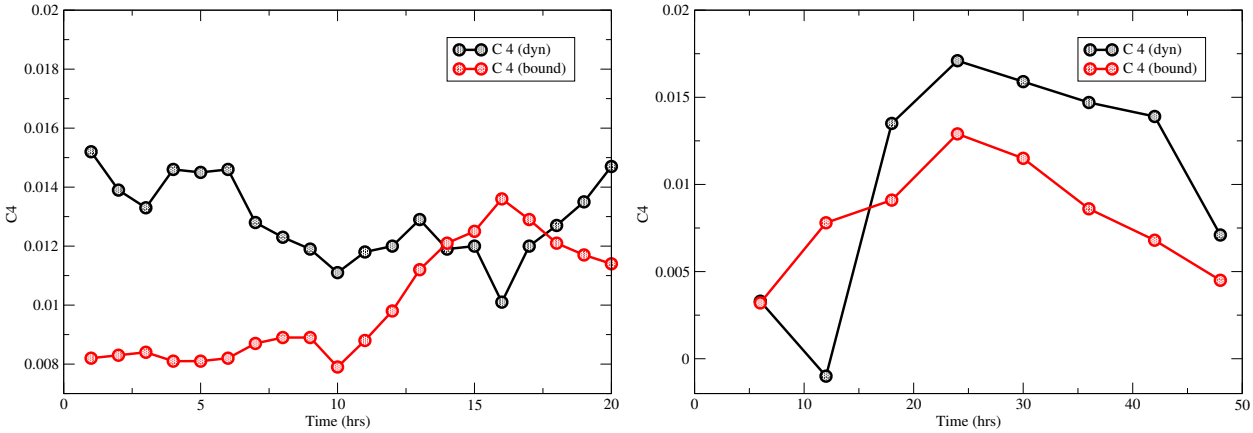

Figure 6: Evolution in time of dynamic and bound-wave part of the kurtosis factor C_4 for the Draupner case (left panel) and the Andrea storm (right panel).

kurtosis only reached a maximum for the Andrea freak wave event. For the Draupner time series the dynamic kurtosis is fairly flat and even reaches a minimum at the time of the freak wave event. To conclude the discussion of the kurtosis time series it is noted that for the Andrea storm the range of kurtosis is quite large and even becomes negative at 12 hrs. At that time the angular width of the wave spectrum is quite large as shown in the spectral plot of Fig. 3. Therefore, dynamic kurtosis has a sensitive dependence on angular width, much more so than the bound-wave part.

Finally, as already pointed out in the Appendix, there is a marked difference between the statistical information derived from the free waves and the bound waves. For given wave spectrum bound-wave skewness and kurtosis are independent of time, whereas the dynamic kurtosis evolves in time. This is shown in Fig. 16 which displays the evolution in time of dynamic kurtosis for a narrow-band wave train, but it is also very much the case for the Draupner freak wave and the Andrea storm using the expression for the kurtosis valid for arbirary spectra. In Fig. 7, I have plotted for all the given simulated spectra the evolution of dynamic kurtosis as function of the dimensionless time $\tau = \delta_\omega^2 \omega_p T$, with $\delta_\omega = \sigma_\omega / \omega_p$. This is the appropriate evolution time scale which follows from the narrow-band considerations in the Appendix. Because realistic spectra are not quite narrow-band I have chosen a relative width of the spectrum which is representative for the whole spectrum. I have therefore chosen the definition of

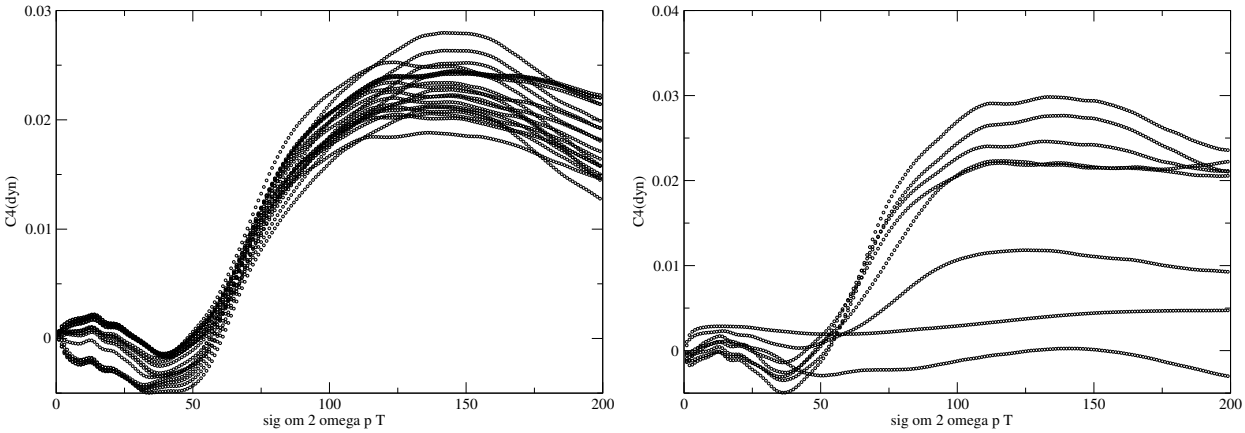

Figure 7: Evolution of dynamic kurtosis κ_{30}^{dyn} as function of the dimensionless time $\tau = \sigma_\omega^2 \omega_p T$, where σ_ω is the relative width of the frequency spectrum and ω_p is the angular peak frequency. Left panel shows the Draupner case while the right panel shows the Andrea storm.

spectral width introduced by Longuet-Higgins (1983), i.e. $\delta_\omega = \nu = (m_0 m_2/m_1^2 - 1)^{1/2}$, see just below Eq. (18). Since in practice δ_ω is of the order of 0.3 the time scale of 200 units in the graph corresponds to 300 wave periods. It is seen that on this relatively long time scale the solution is still smooth, but for longer time scales the solution becomes erratic. In agreement with an earlier remark it is seen that the range in kurtosis values for the Draupner event is fairly small since the left panel of Fig. 7 shows a surprisingly universal time behaviour. However, this is much less the case for the Andrea storm, shown in the right panel, hence the range of kurtosis values is much larger.

The question now is how to deal with the time dependency of the dynamic kurtosis, because I would like to have a simple measure for estimating the severity of the sea state. The most straightforward way to deal with this is to take the mean value of the kurtosis obtained from an average over the whole period shown in the Figure. Note that in the calculations the assumption has been made that initially the dynamic kurtosis vanishes, and, therefore, the Figure basically gives the response of the dynamical wave system to rapid pertubations caused by e.g. a rapid increase of wind or the passage of a frontal system.

3.2 Probability estimates of extreme events using exact computations.

Let us now try to establish how extreme the Draupner and Andrea freak waves are. For the Draupner case Miguel Onorato provided me, by using the Hilbert transform of the actual sea surface elevation time series, with the envelope time series ρ and by using the fact that envelope wave height is twice the envelope it was found that the observed maximum envelope wave height was 3.1 times the significant wave height, or in real terms $h_{max} = 35$ m. For the Andrea storm I had no access to time series so I estimated the maximum envelope wave height by taking twice the maximum crest height, which amounts to 3.26 times the significant wave height (Magnusson and Donelan, 2013). Clearly, we are dealing here with very extreme events.

In order to establish how rare the Draupner and Andrea events are, it should be realized that a wave model gives the ensemble mean of the sea state in a box surrounding the point of interest. This remark is also valid for the probabilities of events, we only know the ensemble average probability distribution function for the envelope wave height, therefore it is not possible to provide estimates of probabilities at a certain location. On the other hand, the statistics (e.g. skewness and kurtosis) derived from a short

observed time series are not representative for the stats of a domain of the size of the chosen resolution. This is readily seen from the Draupner timeseries by estimating the kurtosis factor C_4. It is found that according to the observed time series C_4 is about 0.5 which is 40 times larger than the result from the exact computations presented in the left panel of Fig. 5.

Therefore, one can only answer how likely such an event is, given the spatial resolution of the wave model (in this case 14 km) and given the present knowledge of the physics of freak wave generation. I therefore concentrated on the maximum wave height distribution and I determined the exceedance probability $P_{max}(h_{max} \geq h_{obs})$ that in a domain of 14×14 km such an extreme event occurs. This requires that one needs to count the number of events in a spatial domain. This is not a trivial matter and at the moment results are only known for the surface elevation of a linear sea state which has a Gaussian p.d.f. See for this the work of J. Adler (1981) which has been further discussed by Baxevani and Rychlik (2006) and implemented by Fedele (2012) and Benetazzo *et al.* (2015). In the present case I need to estimate the number of events for a completely different problem, namely for the maximum envelope wave height which obeys in the lowest approximation a Rayleigh distribution, but nonlinear effects related to skewness and kurtosis are important as well. Such an estimate is not available at the moment. For lack of alternatives I have therefore used the Baxevani and Rychlik estimates, and they give for a domain of 14×14 km a surprisingly large number of events, in the order of 500,000 or more.

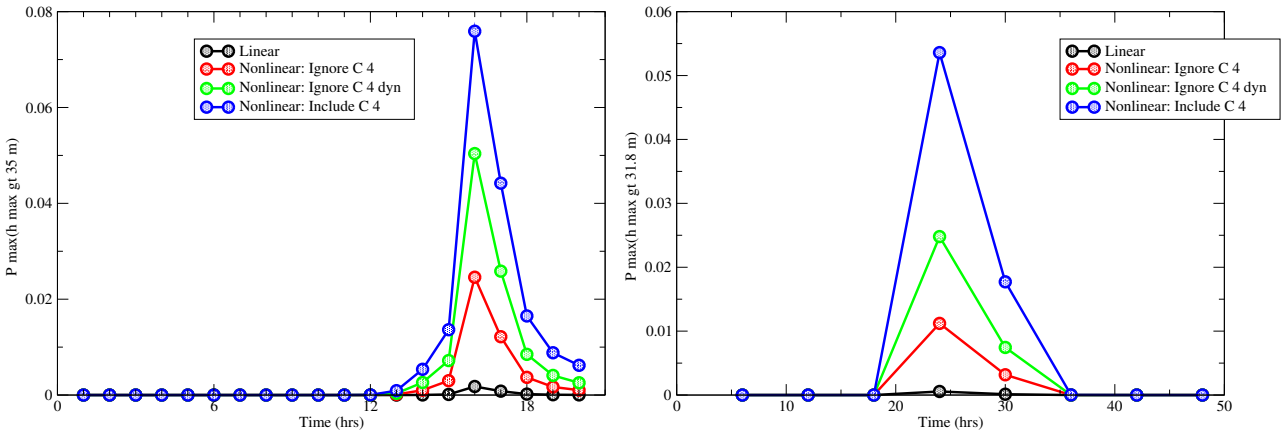

Figure 8: Evolution in time of simulated exceedance probability $P_{max}(h^{obs}_{max})$ for $h^{obs}_{max} = 35$ m (Draupner, left panel) and for $h^{obs}_{max} = 31.8$ (Andrea storm, right panel). For comparison the corresponding results from linear theory are shown, whereas also the impact of dynamic kurtosis and total kurtosis is depicted.

In Fig. 8 the timeseries of exceedance probability $P_{max}(h_{max} \geq h^{obs}_{max})$ for the Draupner freak wave (left panel) and the Andrea storm (right panel) are shown. It is clear that when all nonlinear effects are included that these events are rather plausible as the probabilities are already of the order of 6-8 %, while according to linear theory these extreme events are quite improbable.[1] In the Figure I have also shown exceedance probabilities when dynamic kurtosis is omitted in the calculation and when both dynamic and bound-wave kurtosis are omitted. In particular in the case of the Andrea storm this would result in a considerable reduction of probabilities. For dynamic kurtosis the reduction is a factor of 2 while for total kurtosis the reduction is a factor of 5. All this suggests that it is important to include deviations from Normality caused by finite skewness and kurtosis.

[1] These probabilities can be further enhanced when the time dimension is taken into account as well. Taking a realistic duration of 20 minutes and a peak period of 12 seconds these probabilities are further enhanced by a considerable amount.

3.3 Parametrisation of the bound skewness and kurtosis.

The parametrisations for the bound-wave skewness and kurtosis factors C_3^{bound} and C_4^{bound} have been guided by the narrow band expression (A24) and (A27), presented in the Appendix. This approach seems to work quite well, as will be seen in a moment, because the bound-wave stats are insensitive to the directional width of the wave spectrum. This has been checked numerically for JONSWAP spectra with a variable directional width.

After some trial and error the following parametrisation for the skewness factor C_3 and kurtosis factor C_4 was found:

$$C_3^{bound} = 2.24 m_0^{1/2} (\alpha + \Delta),$$

$$C_4^{bound} = 7.28 m_0 \left\{ \gamma + \alpha^2 + (\alpha + \Delta)^2 \right\}, \tag{33}$$

where the wavenumber and depth dependent parameters α, γ and Δ are defined in Eq. (A20) and m_0 is the zeroth moment of the frequency spectrum. It is noted that it is important to choose as wavenumber a characteristic wavenumber that reflects that the wave spectrum is broad-banded. As a first guess I tried to choose a characteristic wavenumber $\bar{k}$ that follows from the inverse of the dispersion relation $a\bar{\omega} = \omega(\bar{k}, h)$, where $\bar{\omega} = m_0/m_{-1}$ and a is a tuning parameter. Results for skewness and kurtosis are very sensitive to the choice of this tuning parameter. In the end I settled for the choice $a = 0.9$ which, for deep-water waves, implies that the characteristic wavenumber $\bar{k}$ is larger by about 25% when compared to the peak wavenumber k_p. Thus, in the formulae for α, γ and Δ, for example, the wave number k_0 is replaced by $\bar{k}$, while, to be consistent, this is also done for all wave number dependent factors in the dynamic kurtosis parametrisation of the next section.

These parametrisations compare very favourably with the exact computations from the Draupner and Andrea cases, as shown in the scatter plots of Fig. 9.

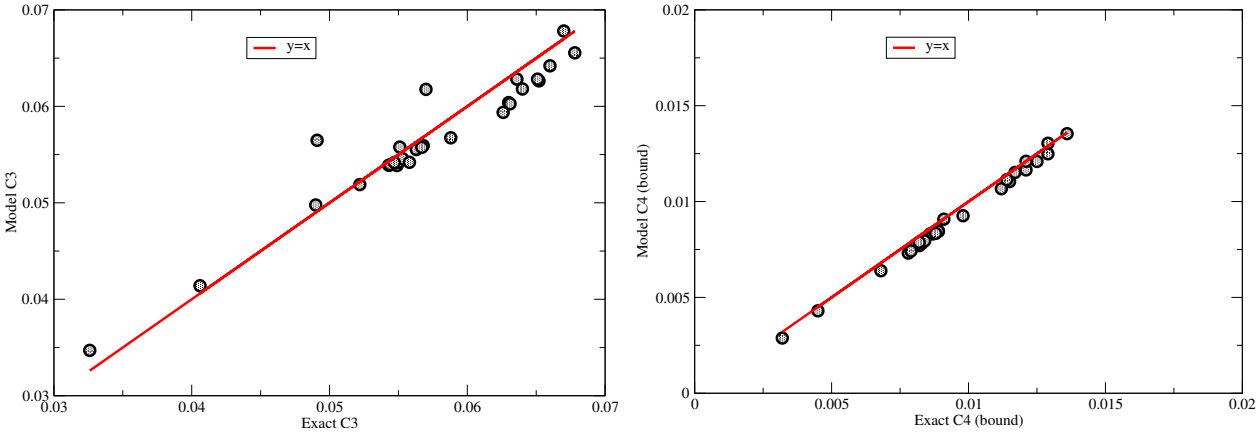

Figure 9: The left panel shows the comparison of parametrized skewness factor C_3^{bound} against exact computation from the Draupner and Andrea events, while the right panel shows the comparison for the kurtosis factor C_4^{bound}.

Quantitatively, the agreement is impressive as follows from a linear fit of parametrized results against exact computations which gives correlations of more than 96%. Nevertheless, it is noted that the scatter-plot of the skewness factor shows two modest outliers which correspond to the broad angular distribution cases of the Andrea storm.

3.4 Parametrisation of the dynamic kurtosis.

The parametrization of the dynamic part of the kurtosis has been guided by the definition (A15) and the narrow-band result (A17), which is strictly speaking only valid for Gaussian spectra and gives an estimate of the maximum of dynamic kurtosis. Rather then the maximum value to estimate the severity of the sea state, I will use its average value over a time span of about 300 wave periods, as already suggested when discussing Fig. 7. I have tried to stay as close as possible to the narrow-band result, and I paid particular attention to the replacement of the definitions of the Benjamin-Feir Index and the ratio of the square of directional width and frequency width to appropriate forms for broad-banded spectra.

After some extensive trial and error I arrived at the following results: The dynamic kurtosis factor is given by

$$C_4^{dyn} = J(R)BFI^2, \tag{34}$$

where

$$J(R) = NR_0\frac{(\alpha - R)}{R + R_0},\ N = \frac{\pi}{3\sqrt{3}}, \tag{35}$$

with $R_0 = 7.44\sqrt{3}/4\pi^3$. The threshold value for R, indicating a change in sign of the dynamic kurtosis, is given by $\alpha = 1.1$. The Benjamin-Feir Index is defined in Eq. (A13), where the relative angular frequency width is obtained from Goda's peakedness factor Q_p defined as

$$Q_p = \frac{2}{m_0^2}\int_{\mathscr{D}} \mathrm{d}\omega\ \omega E^2(\omega), \tag{36}$$

with $E(\omega)$ the angular frequency spectrum and the integration domain $\mathscr{D}$ consists of all frequencies for which $E(\omega) > E(\omega_p)/4$ (Janssen and Bouws, 1986). The relative angular frequency width δ_ω then follows from

$$\delta_\omega = \frac{1}{Q_p\sqrt{\pi}}. \tag{37}$$

This definition of width emphasizes the peak region of the wave spectrum, which is thought to control the Benjamin-Feir instability. In practice, it turns out, however, that with this definition of Q_p noisy results are obtained. It was therefore decided to integrate over the whole frequency domain $E(\omega) > 0$ and to reduce the result by a factor 0.65 to mimic the original definition of Q_p.

In the Benjamin-Feir Index the steepness of the waves is given by $\varepsilon = \bar{k}m_0^{1/2}$. The characteristic wave number $\bar{k}$ is also used in the depth dependent factor of (A13).

Finally, the parameter R which is basically measuring the importance of directional width with respect to the frequency width is given in Eq. (A14). Here, the directional width is determined according to Eq. (32), while, as the damping of the Benjamin-Feir instability is caused by the broad-band aspects of the wave spectrum, the relative frequency width is given by $\delta_\omega = \nu = (m_0m_2/m_1^2 - 1)^{1/2}$, where $m_n, n = 0, 1, 2$ are the moments of the frequency spectrum. A comparison of the results obtained from the above parametrization and the exact computations using spectra from the Draupner and Andrea events is shown in the left panel of Fig. 10. There is a fair agreement but, clearly, compared to for example the bound-wave kurtosis, the agreement is not as good. Fortunately, the probability calculations only involve the total kurtosis, and as shown in the right panel of Fig. 10, this shows a better agreement with correlations of 91%.

As an important check I have compared in Fig. 11 exceedance probabilities obtained with the parametrisations for skewness and kurtosis with the exact calculations and a satisfactory agreement is to be noted.

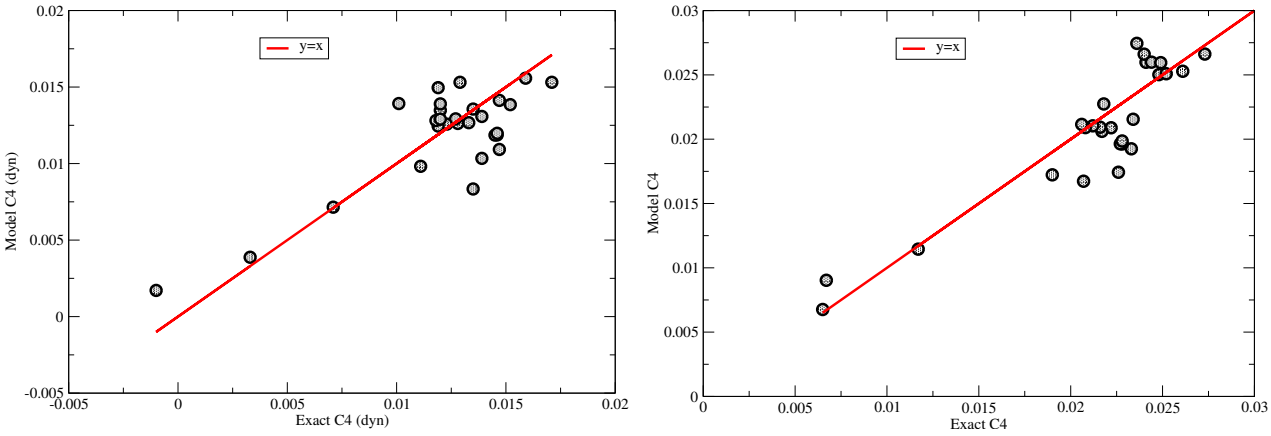

Figure 10: The left panel shows the comparison of parametrized dynamic kurtosis factor C_4^{dyn} against exact computations using spectra from the Draupner and Andrea events, while the right panel shows the comparison for the total kurtosis factor C_4.

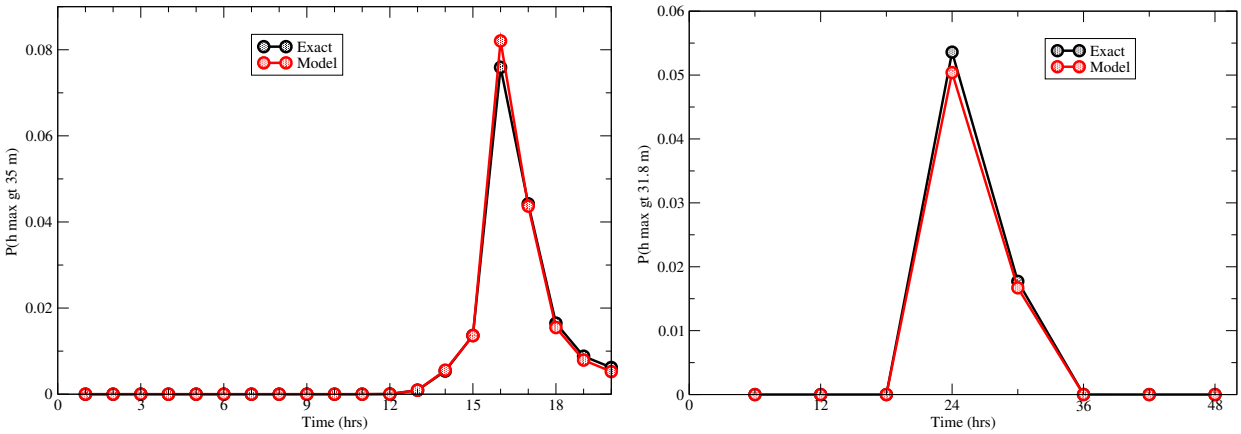

Figure 11: Comparison of parametrized exceedance probability $P_{max}(h_{max}^{obs})$ for $h_{max}^{obs} = 35$ m (Draupner, left panel) and for $h_{max}^{obs} = 31.8$ (Andrea storm, right panel) with numerical computations using the exact theory.

4 Pre-operational results.

The final step I have taken is to check results of the here obtained parametrizations for skewness and kurtosis in the context of the ECWAM wave prediction system. Firstly, I have studied results from a single grid-point wave model in deep and shallow water which illustrates the sensitive dependence of the dynamic kurtosis on the normalized directional width R. Secondly, I have obtained statistical results using forecast ECWAM spectra from one synoptic time and I have studied relations such as the dependence of skewness and kurtosis on the wave age parameter c_p/U_{10} and the dependence of the normalized maximum envelope wave height on the Benjamin-Feir Index and the dimensionless directional width R.

4.1 Single gridpoint Results.

The parametrization of the dynamic kurtosis is given in Eqns. (34) and (35). It shows that dynamic kurtosis depends on the square of the Benjamin-Feir Index BFI appropriately defined by including shal-

low water effects. In addition, it shows that dynamic kurtosis reduces when, compared to the frequency width, the directional width of the 2D wave spectrum increases, where the effect of directional width is measured by the dimensionless directional width R. Suppose that initially the wave spectrum has a narrow directional distribution such that $R < \alpha$. Then, the nonlinear interactions will broaden the directional spectrum in such a way that R increases and hence the dynamic kurtosis decreases until for large time an 'equilibrium' condition is obtained for which the dynamic kurtosis vanishes. Therefore, large deviations from the Gaussian equilibrium, and hence large values of kurtosis, are only expected for relatively short times.

In order to illustrate the sensitive dependence of results from dynamic kurtosis on the dimensionless width R, I have run the one-gridpoint version of the WAM model for deep-water and shallow water (with depth of 40 m). The windspeed was constant and had the value of 18.45 m/s. The wave spectrum was discretized in the same manner as the operational ECWAM model and therefore consisted of 36 frequencies and 36 directions. As initial condition a JONSWAP spectrum was chosen with a cos-square directional distribution. The directional distribution is so broad that dimensionless directional width is larger than the threshold value α, hence dynamic kurtosis is initially negative. In Fig. 12, two results are shown from this experiment, namely a comparison of the evolution in time of the dimensionless angular width of the spectrum for the deep and the shallow water case and the consequent evolution of the dynamic kurtosis. It is noted that shallow water effects may play an important role in the formation

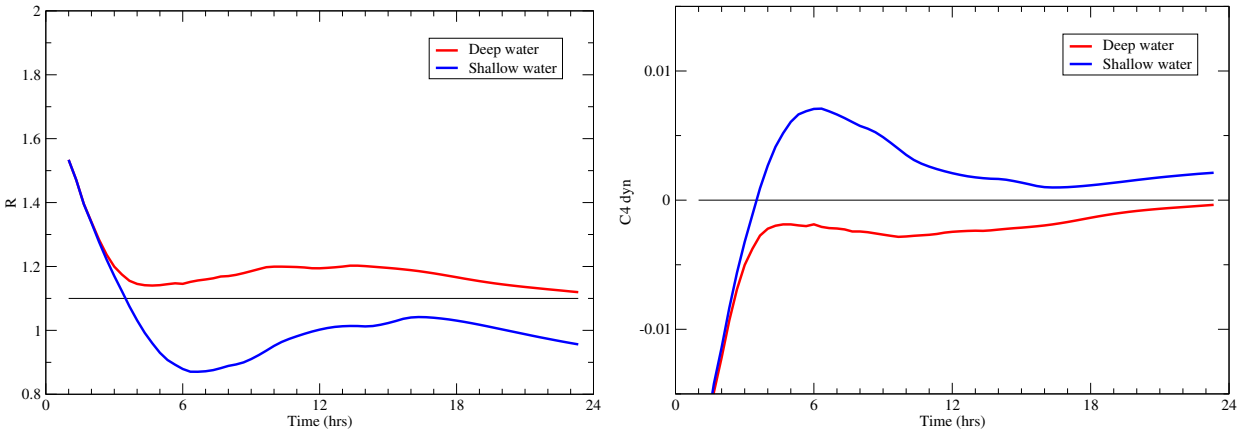

Figure 12: Left Panel: Comparison of time-evolution of normalized width parameter R for deep and shallow water. The threshold value of $\alpha = 1.1$ is indicated as well. Right panel: Comparison of time-evolution of dynamic kurtosis for deep and shallow water.

of freak waves as in deep-water the dynamic kurtosis is negative resulting in a small defocussing of the weakly nonlinear wave train, while in shallow water the wave train experiences focussing because the dynamic kurtosis is positive after time equals 3 hours. Inspecting the time evolution of the normalized width R it should be clear that this different behaviour in deep and shallow water is connected to the findings in Section 3 that shallow water spectra are, compared to deep water, more narrow. This has, according to the left panel of Fig. 12 important consequences because for deep water R is always larger than the threshold value of R, while in shallow water R gets below the threshold value, giving focussing.

4.2 A Synoptic Example.

As a final illustration of the properties of the new version of the freak wave warning system results of a single forecast, namely the one-day forecast of the 19th of December 2017, will be briefly discussed.

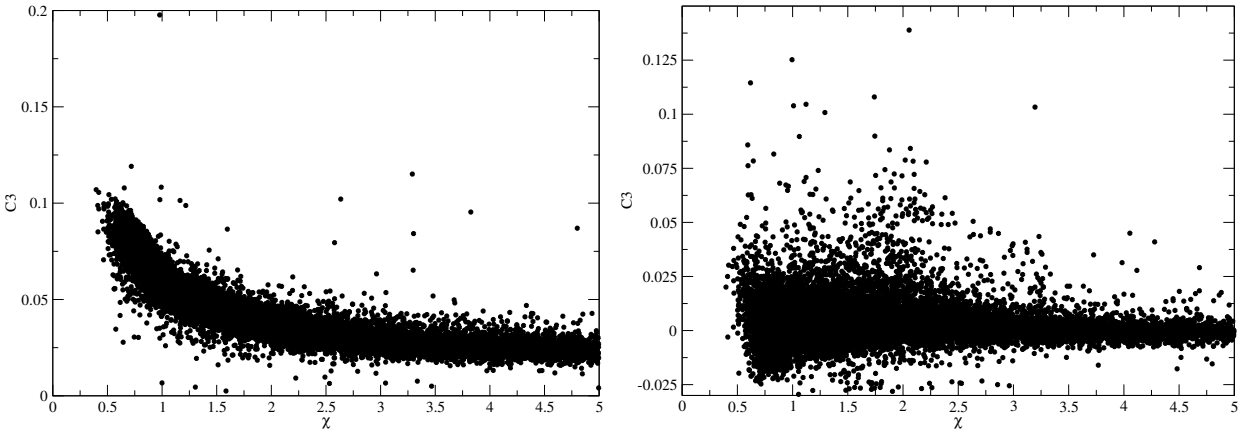

Figure 13: Skewness factor C_3 (left panel) and kurtosis factor C_4 (right panel) versus wave age parameter $\chi = c_p/U_{10}$. Note that there are many occasions where the directional wave spectrum is so broad that kurtosis is slightly negative.

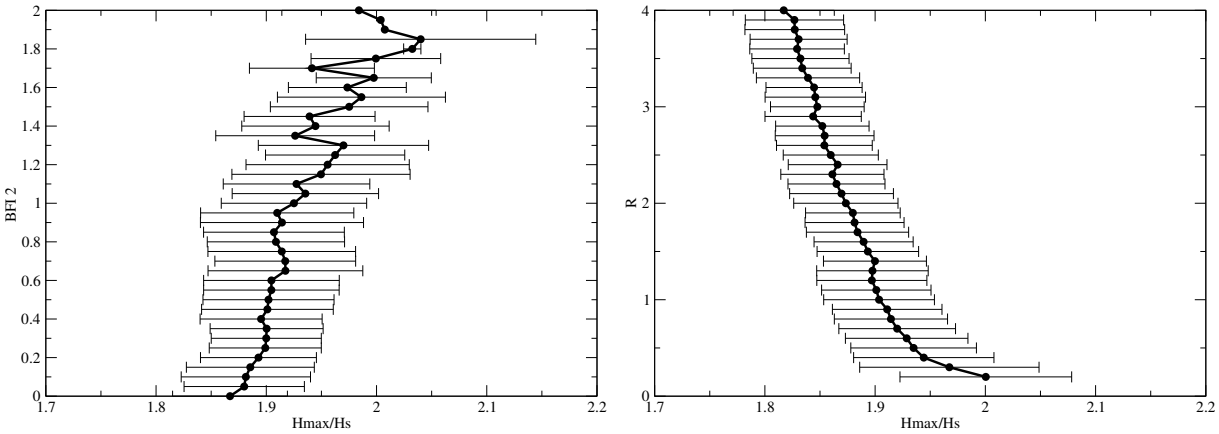

Figure 14: Left Panel: Dependence of expectation value of normalized maximum wave height on the square of the Benjamin-Feir Index (left panel) and on normalized directional width R (right panel). The error bars give the width of the maximum wave height distribution at the BFI^2 or R value of interest

A number of integral parameters such as significant wave height and several versions of mean period were retrieved which allowed the determination of the moments m_{-1}, m_0, m_1, m_2 needed for the specification of the spectral frequency width parameters. In addition, parameters such as the Benjamin-Feir Index and the angular width were retrieved, enabling the determination of the skewness and kurtosis at every gridpoint and also the determination of the expectation value of maximum envelope wave height.

In Fig. 13, results for skewness and kurtosis from a one-degree retrieval are plotted as function of a parameter measuring the stage of development of the sea state, namely the wave age $\chi = c_p/U_{10}$. For young waves, with $\chi < 1$ the envelope skewness C_3 reaches values of 0.1 which corresponds to a surface elevation skewness which is three times larger. The behaviour of the kurtosis parameter C_4 which is the sum of bound-wave kurtosis and dynamic kurtosis is somewhat more complex. Although the bound-wave part of kurtosis is always positive, dynamic kurtosis may become negative, which occurs for spectra with a broad directional distribution. As a consequence, in many cases (50% or more) kurtosis turns out to be negative, giving compared to the Gaussian sea state a reduced risk of the occurence of freak waves. On the other hand, for narrow directional spectra, kurtosis is positive, reaching values of up to 0.1, resulting

in an enhanced risk for freak waves. Note that these large values of kurtosis are caused by the dynamic part of kurtosis. If one would disregard the dynamic part in the kurtosis calculation than kurtosis would always be positive but would reach at most values of 0.02.

In the next plot, Fig. 14, I concentrate on the expectation value of maximum envelope wave height for a 20 min. time series and I study its dependence on parameters such as the square of the Benjamin-Feir Index, BFI^2, and the dimensionless directional width R. These relations are obtained by collecting maximum envelope wave height data as function of a discretized version of the independent parameter and by plotting the bin-average. In agreement with expectations and with results of Burgers *et al.* (2008), based on observations of normalized maximum wave height obtained from AUK platform in the central North Sea, the expectation value of maximum envelope wave height is seen to increase with increasing Benjamin-Feir Index. On the other hand, maximum wave height is seen to decrease, as expected, with increasing dimensionless directional width.

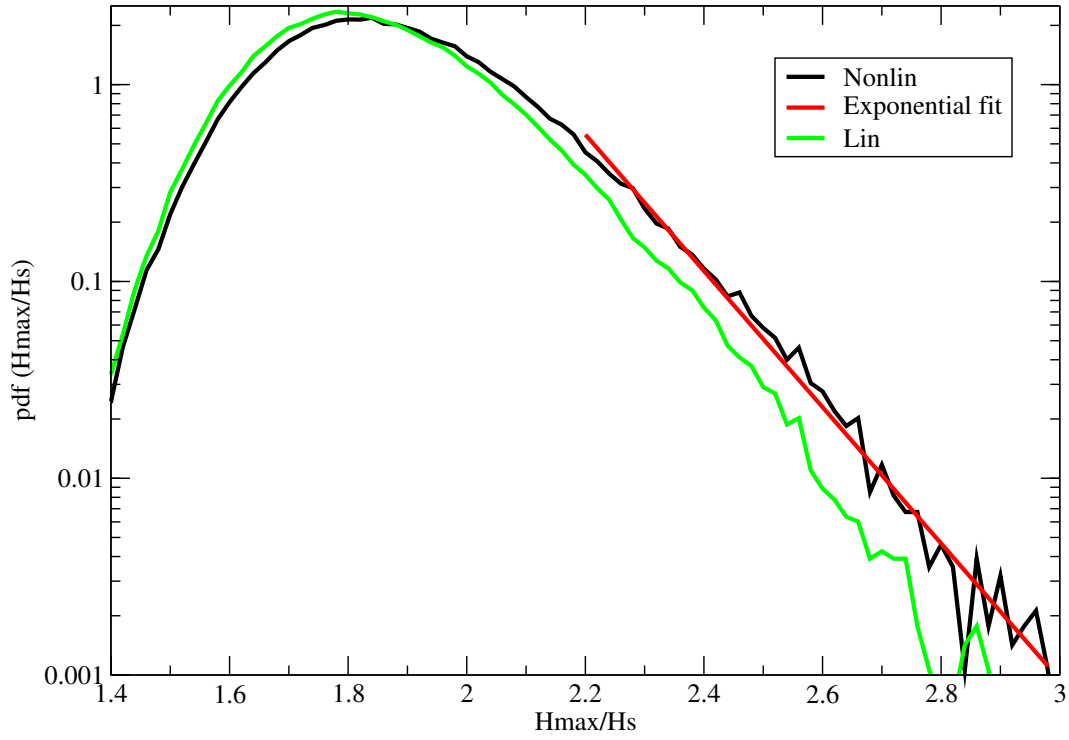

Figure 15: Global maximum wave height distribution obtained by a random draw of H_{max} for given number of waves and given skewness and kurtosis. Including skewness and kurtosis shows that the tail of the distribution is exponential. The distribution according linear theory is shown as well.

Furthermore, in Janssen and Bidlot (2009) a detailed comparison between observed and modelled distribution of maximum envelope wave height has been made. As argued by these authors, a way to simulate the observed maximum wave height distribution is to start from the theoretical pdf of maximum wave height, the explicit form of which is given in Eqns. (23)-(25), and to generate from this pdf for given number of waves N_{slc} and given skewness C_3 and kurtosis C_4 a random draw of maximum wave height. The usual procedure for this is that one obtains a random draw of maximum envelope wave height from the condition that the cumulative distribution is a random number between 0 and 1. The resulting modelled distribution function is plotted in Fig. 15. It is remarked that the tail of the maximum wave height distribution is basically the number of degrees of freedom N (see (25)) times the envelope wave height pdf (22). Therefore, for large values of maximum envelope wave height the distribution function is an exponential. As can been seen from the present fit, the simulated maximum wave height distribution

closely follows the exponential fit, which on a logarithmic plot is a straight line. In order to illustrate effects of nonlinearity, also simulated maximum wave height distribution without nonlinear effects is shown, and clearly, nonlinear effects are seen to play an important role for the extreme events.

Finally, the present approach has been based on an analysis of time series using the envelope. This differs from the usual method whereby one considers wave height or crest height. In these latter approaches an extreme event is called a freak if wave height is larger than 2.2 times the significant wave height or, alternatively, if the crest height is larger than 1.25 times the significant wave height. In my opinion, the envelope waveheight follows closely the crest of the waves and therefore, in the context of the envelope approach, I would call an extreme event a 'freak' if the maximum envelope wave height is 2.5 times the significant wave height $H_S = 4\sqrt{m_0}$ with m_0 the zeroth moment of the wave spectrum. Adopting this definition of a freak wave it is therefore of interest to determine the probability that maximum normalized envelope wave height is larger than 2.5. Based on the Global distribution shown in Fig. 15, this probability is according to linear theory about 2.5×10^{-3} while according to nonlinear theory, this probability is a factor of 2.5 larger, namely 6.6×10^{-3}.

5 Conclusions.

An overview is presented of the theoretical probablistic approach of extreme events, which focusses on the statistical properties of wave energy. Here, wave energy is measured from timeseries of the wave envelope, where the wave envelope is obtained from the surface elevation time series η and the corresponding Hilbert transform ζ. For such a signal, the envelope wave height distribution may be obtained using as starting point the characteristic function of surface elevation and its Hilbert transform. This approach has a restricted range of validity and in order to capture really extreme events an exponential tail has to be added. A procedure to accomplish this has been proposed and results have been validated against Monte Carlo simulations (Janssen, 2015b).

A key quantity to characterize extreme events is the p.d.f. for maximum envelope wave height. Here it is shown that, based on a comparison with Monte Carlo simulations, for envelope wave height the most appropriate approach is the one suggested by Naess (1982). This approach has the added advantage that with the stretched exponential distribution a really simple expression for the expectation value of maximum envelope wave height may be obtained.

In the Appendix a brief overview is given of the analytical formulation of statistical quantities such as skewness and kurtosis in terms of multi-dimensional integrals involving the combination of interaction coefficients and wave spectra. Numerical evaluation of these integrals is in principle possible but requires a considerable amount of computing power (On my PC the evaluation of the stats for the Draupner case and the Andrea event took 2 hours). For an operational implementation parametrization of the skewness and kurtosis is highly desirable. In this note I have developed such a parametrization of the wave stats and a satisfactory agreement with the computations using the analytical theory has been obtained.

The time series for the exceedance probabilities of maximum wave envelope height suggest that for an area of the size of the resolution of the wave model it is plausible that the Draupner wave and the Andrea event did happen. In addition, knowledge of the deviations from Normality as expressed by skewness and kurtosis play an important part in 'explaining' these events. It is emphasized once more that for a quantity such as envelope wave height it is essential that effects of of both bound-wave and dynamic kurtosis need to be included.

In fact, at first I was somewhat surprized that dynamic kurtosis played such an important role in the

freak wave events discussed in this note. First of all, with the work of Janssen and Onorato (2007) in mind, one would expect that the Benjamin-Feir instability plays a relatively minor role for surface gravity waves in intermediate water depth, because the relevant interaction coefficient vanishes for $kh = 1.363$ and changes sign for even lower dimensionless depth. However, this is only true for one-dimensional modulations. Hayes (1973) has shown that for two-dimensional modulations there is always instability, though in practice growthrates are vanishingly small for $kh < 0.5$. The consequences of this are discussed in Appendix B, resulting in a parametrization of the nonlinear interaction coefficient that depends explicitely on spectral width in frequency direction space. The upshot is that even for shallow water waves Benjamin-Feir instability may exist and may give a finite contribution to the kurtosis of the sea state.

Secondly, in intermediate water depth wave spectra are much more narrow in direction than in the deep water case. This follows from a plot of the spectra which suggests that the directional distribution of the spectra in waters with dimensionless depth $k_p h = 1.5 - 2$ is much narrower. And experimentation with the single-gridpoint model suggests that the cause for the narrower spectra is connected to the bottom friction term. Perhaps, bottom friction, which mainly affects and removes energy from the long waves, disrupts the normal nonlinear energy fluxes in the spectrum to the the long waves to such an extent that the widening of the angular distribution by the nonlinear transfer is halted. However, more work is required to better understand the role of bottom friction in the formation of the directional distribution.

Finally, it should be pointed out that, if desired, a very similar approach may be applied to obtain the statistical properties of the surface elevation. However, the details will be different. For example, the maximum surface elevation distribution can be described adequately by means of the method suggested by Goda (2000) but it is still not clear yet how to add an exponential tail to the nonlinear p.d.f. of the surface elevation. Clearly, more research is required to accomplish this.

Appendices.

A Skewness and Envelope kurtosis.

As already discussed in Mori and Janssen (2006) and Janssen (2009) skewness and kurtosis consists of two contributions, one from the free waves and one from the bound waves. The properties of these contributions differ from each other and therefore they will be discussed separately. For example, while it is straightforward to obtain the narrow-band limit of the bound-wave part of skewness and kurtosis, this is not possible for the free-wave part of the (envelope) kurtosis as for the latter the narrow-band limit does not exist. Therefore, a different approach needs to be followed in order to obtain simplified expressions for the free-wave part of the kurtosis. In contrast to the bound-wave case, it is found that the free-wave contribution to kurtosis has a sensitive dependence on spectral shape, it depends, in particular, on the directional and frequency width.

Following Janssen (2014) we perform a time series analysis in order to evaluate quantities such as the variance of the surface elevation η and its Hilbert transform ζ and a number of skewness terms and the envelope kurtosis. Recall that

$$\eta = \frac{1}{2}(Z + Z^*), \text{ and } \zeta = \frac{1}{2i}(Z - Z^*),$$

where (see Janssen, 2014) the complex function Z is obtained from the canonical transformation by collecting together terms of similar time-asymptotic behaviour, i.e. Z contains all the terms that vanish for $\Im(t) \to -\infty$. The canonical transformation is only known as an expansion in steepness ε so we write $Z = \varepsilon Z_1 + \varepsilon^2 Z_2 + \varepsilon^3 Z_3$ with

$$Z_1 = 2\int_{-\infty}^{\infty} \mathrm{d}\mathbf{k}_1 \, f_1 a_1 \, e^{i\theta_1}, \tag{A1}$$

where $f_1 = (\omega_1/2g)^{1/2}$, $\theta_1 = \mathbf{k}_1 \cdot \mathbf{x}$, and

$$Z_2 = 2\int_{-\infty}^{\infty} \mathrm{d}\mathbf{k}_{1,2,3} \, f_2 f_3 \, e^{i\theta_1} \left\{ \mathscr{A}_{2,3} a_2 a_3 \delta_{1-2-3} + 2\mathscr{B}_{2,3} a_2^* a_3 H_{3-2} \delta_{1+2-3} \right\}, \tag{A2}$$

while

$$\begin{aligned} Z_3 = 2\int \mathrm{d}\mathbf{k}_{1,2,3,4} f_2 f_3 f_4 e^{i\theta_1} \{ & \mathscr{D}_{1,2,3,4} a_2 a_3 a_4 \delta_{1-2-3-4} + \mathscr{C}_{1,2,3,4} a_2 a_3 a_4^* \delta_{1-2-3+4} H_{2+3-4} \\ & + \mathscr{C}_{-1,2,3,4} a_2^* a_3^* a_4 \delta_{1+2+3-4} H_{4-3-2} \}. \end{aligned} \tag{A3}$$

The interaction coefficients $\mathscr{A}, \mathscr{B}, \mathscr{C}$, and $\mathscr{D}$ are defined in Janssen (2009). The Heaviside function $H(x)$ is defined in such a way that $H(0) = 1/2$ and in the above formulae the argument of the Heaviside function is a sum of angular frequencies, e.g. $H_{3-2} = H(\omega_3 - \omega_2)$. Note that the term Z_1 represents the contribution of the free waves to the surface elevation, while the terms Z_2 and Z_3 represent the contributions by the bound waves. Therefore, the free-wave contribution to skewness and kurtosis is determined by the statistical properties of Z_1, while the other two terms are required to determine the contributions to bound-wave statistics.

The third and fourth cumulants of surface elevation η and its Hilbert transform ζ are defined as follows: The third cumulants are

$$\kappa_{30} = \frac{\langle \eta^3 \rangle}{\langle \eta^2 \rangle^{3/2}}, \; \kappa_{21} = \frac{\langle \eta^2 \zeta \rangle}{\langle \eta^2 \rangle \langle \zeta^2 \rangle^{1/2}}, \; \kappa_{12} = \frac{\langle \eta \zeta^2 \rangle}{\langle \eta^2 \rangle^{1/2} \langle \zeta^2 \rangle}, \; \kappa_{03} = \frac{\langle \zeta^3 \rangle}{\langle \zeta^2 \rangle^{3/2}}, \tag{A4}$$

while the relevant fourth cumulants are given by

$$\kappa_{40} = \frac{\langle \eta^4 \rangle}{\langle \eta^2 \rangle^2} - 3, \; \kappa_{22} = \frac{\langle \eta^2 \zeta^2 \rangle}{\langle \eta^2 \rangle \langle \zeta^2 \rangle} - 1, \; \kappa_{04} = \frac{\langle \zeta^4 \rangle}{\langle \zeta^2 \rangle^2} - 3, \tag{A5}$$

The procedure to obtain explicit expressions for the cumulants is straightforward but laborious. One substitutes the expressions for η and ζ into the above definitions and evaluates for the bound waves the relevant integrals under the assumption of a homogeneous, Gaussian ocean surface. In order to find a non-trivial result for the free waves one needs to obtain from the evolution equation of the free waves the contribution of the fourth order cumulants, as detailed in Janssen (2003).

A.1 Free Waves.

The free wave case has been discussed extensively by Mori and Janssen (2006). For the free waves the skewness vanishes while the kurtosis enjoys certain symmetry properties in such a way that $\kappa_{04} = \kappa_{40}$ while $\kappa_{22} = \kappa_{40}/3$. Therefore, using (5) and (4) one finds

$$C_4^{free} = \frac{1}{3} \kappa_{40}^{dyn}, \tag{A6}$$

where κ_{40}^{dyn} is explicitely given by Janssen (2003) in terms of the directional angular frequency spectrum $E(\omega, \theta)$, i.e.

$$\kappa_{40}^{dyn} = \frac{12g}{m_0^2} \int \mathrm{d}\theta_{1,2,3} \mathrm{d}\omega_{1,2,3} T_{1,2,3,4} \sqrt{\frac{\omega_4}{\omega_1 \omega_2 \omega_3}} \times G(\Delta\omega, t) E_1 E_2 E_3. \tag{A7}$$

Here, $G(\Delta\omega, t)$ is the time-dependent real part of the resonance function, defined by

$$G(\Delta\omega, t) = \frac{1 - \cos(\Delta\omega t)}{\Delta\omega},$$

while the frequency mismatch $\Delta\omega$ is given by $\Delta\omega = \omega_1 + \omega_2 - \omega_3 - \omega_4$, and the fourth wave number follows from the resonance condition in wave number space, i.e. $\mathbf{k}_4 = \mathbf{k}_1 + \mathbf{k}_2 - \mathbf{k}_3$. The frequency ω_4 is obtained by evaluating the dispersion relation at the fourth wavenumber. Eq. (A7) gives the evolution in time of the dynamic part of the kurtosis for given wave spectrum. In general no solution is known so a numerical evaluation of this six-dimensional integral is required. I have written software to calculate κ_{40}^{dyn} for arbitrary spectra and arbitrary depth h under the restriction that $k_p h > 1$. The software has been validated for a number of special cases of which the solution is known, namely for Gaussian spectra in the narrow-band approximation.

It should be realized that Eq. (A7) is quite expensive to evaluate because it involves a six-dimensional integral. With a resolution of 36 frequencies and 36 directions we are looking at $36^6 = 2.18$ Billion evaluations of the transfer coefficient which is quite substantial. For this reason I inspected before hand the simulated spectra of the Draupner case. It turns out that a large part of the frequency-direction space contained small values so that I filtered the evaluation of the integrals accordingly. This filtering operation reduced the number of evaluations of the transfer coefficient to about 11 million. Therefore, for a limited number of spectra, the filtering operation makes numerical evaluation of the free wave kurtosis feasible.

Another point to mention is that the evaluation of the integral involving a rapidly varying resonance function G is very difficult. For large times the time behaviour becomes erratic although there is, in the case of general spectra, no criterium available when the numerical solution becomes seemingly chaotic. In practice, I simply plotted the solution as a function of time and inspected by eye whether the solution was smooth or not.

A.1.1 The narrow-band approximation.

Nevertheless, in operational applications the numerical evaluation of the six-dimensional integral is far too expensive, and an efficient approximation is highly desirable. This efficient approximation is found using the narrow-band approximation applied to Eq. (A7). In this approximation most of the wave energy is concentrated around the carrier wave number k_0, so that the wave spectrum has a small relative frequency width $\delta_\omega = \sigma_\omega/\omega_0$ and a small angular width δ_θ. For surface gravity waves on water of finite depth h the dispersion relation for the carrier reads

$$\omega_0 = \sqrt{gk_0T_0},\ T_0 = \tanh x,\ x = k_0h, \tag{A8}$$

while the first and second derivative become

$$v_g = \omega_0' = \frac{1}{2}c_0\left\{1+\frac{2x}{\sinh 2x}\right\},\ c_0 = \frac{\omega_0}{k_0}, \tag{A9}$$

and

$$\omega_0'' = -\frac{g}{4\omega_0k_0T_0}\times\Omega'', \tag{A10}$$

with

$$\Omega'' = \left\{T_0 - x\left(1-T_0^2\right)\right\}^2 + 4x^2T_0^2\left(1-T_0^2\right). \tag{A11}$$

Note that for any value of the depth h the second derivative is always negative. Finally, the narrow-band limit of the nonlinear interaction coefficient is given by

$$T_{0,0,0,0}/k_0^3 = X_{nl} = \frac{9T_0^4-10T_0^2+9}{8T_0^3} - \frac{1}{x}\left\{\frac{\left(2v_g-c_0/2\right)^2}{c_S^2-v_g^2}+1\right\} + \frac{\kappa_1\nu_1}{\mu_1k_0^3}\frac{\delta_\theta^2}{\delta_\theta^2+\alpha_\omega\delta_\omega^2} \tag{A12}$$

with κ_1, ν_1 and $\mu_1 = c_S^2$ wavenumber and depth dependent coefficients given in (B6), $c_S = \sqrt{gh}$ the shallow water wave velocity and

$$\alpha_\omega = \frac{c_0^2}{v_g^2}\left(1-\frac{v_g^2}{c_S^2}\right).$$

Note that the interaction coefficient consists of three terms. The first two terms are well-known (see e.g. Whitham, 1974) as the first term is connected with the nonlinear dispersion relation for surface gravity waves, while the second term is due to effects of wave-induced current caused by one-dimensional, longitudinal modulations. These two terms are of definite sign so they may cancel each other, which, in fact, happens for $x = k_0h = 1.363$. The third term is new and is connected to the wave-induced current caused by two-dimensional modulations. It also has a definite sign and tends to reduce the dimensionless depth where the nonlinear interaction coefficient vanishes. A complete derivation of this new term and some discussion is presented in Appendix B. Hence, for intermediate water depth waves the nonlinear interactions are, because waves are two-dimensional, still expected to play a relatively important role.

In the narrow-band approximation, the evolution of the kurtosis is determined by two dimensionless parameters. The first one is the shallow water extension of the Benjamin-Feir index. Introducing the wave steepness $\varepsilon = k_0\sqrt{m_0}$, with m_0 the variance of the surface elevation, while δ_ω is the relative frequency width, the Benjamin-Feir Index BFI is defined as

$$BFI^2 = \frac{8\varepsilon^2}{\delta_\omega^2}\times\left(\frac{v_g}{c_0}\right)^2\times\frac{T_0}{\Omega''}\times X_{nl} \tag{A13}$$

Note that in the deep-water limit one recovers the usual expression for the Benjamin-Feir Index, as $\lim_{k_0 h\to\infty} BFI^2 = 2\varepsilon^2/\delta_\omega^2$.

The second dimensionless parameter measures the importance of directional width δ_θ with respect the frequency width δ_ω. In deep water it is defined as $R = \delta_\theta^2/2\delta_\omega^2$ while in general one has

$$R = 4\frac{\delta_\theta^2}{\delta_\omega^2} \times \left(\frac{v_g}{c_0}\right)^3 \times \frac{T_0^2}{\Omega''} \tag{A14}$$

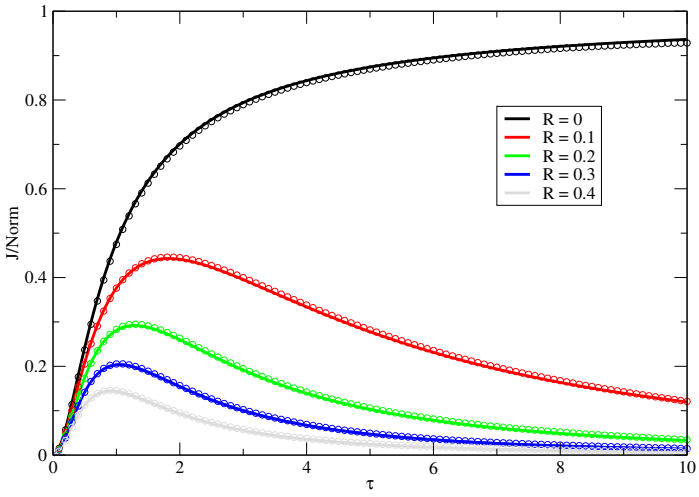

Figure 16: Evolution of normalized kurtosis versus time for different values of R. Results using the numerical solution of (A15) are shown as the full lines, while the circles denote the analytical solution from Fedele (2015).

Applying now the narrow-band approximation to Eq. (A7) the parameter C_4^{free} becomes

$$C_4^{free} = J(R,\tau)BFI^2, \tag{A15}$$

where

$$J(R,\tau) = 2\int \mathrm{d}\nu_{1,2,3}\mathrm{d}\phi_{1,2,3}E_1E_2E_3G(\Delta\omega,\tau), \tag{A16}$$

with resonance function $G(\Delta\omega,\tau) = (1-\cos(\Delta\omega\tau)/\Delta\omega$. Here, $\tau = \delta_\omega^2\omega_0 t$ is dimensionless time, and $\Delta\omega = (\nu_3-\nu_1)(\nu_3-\nu_2) - R(\phi_3-\phi_1)(\phi_3-\phi_2)$. The frequency parameter ν and direction parameter ϕ have been made dimensionless by means of the frequency width and the directional width.

For a Gaussian spectrum

$$E_1 = \frac{1}{2\pi}e^{-\frac{1}{2}(\nu_1^2+\phi_1^2)},$$

the integral in Eq. (A16) may be solved exactly (see e.g. Fedele (2015)) and the resulting solution for different values of R as a function of dimensionless time τ has been plotted in Fig. 16. Note that in the plot the parameter J has been normalized with the factor $\pi/3\sqrt{3}$ which is the time-asymptotic value of J for $R = 0$.

From the plot it is clear, that, except for the case of uni-directional propagation (i.e. $R = 0$), the parameter J and therefore the kurtosis parameter C_4^{free} has a maximum at the finite time $\tau_{max} = 1/(3R)^{1/2}$ after which it decays to zero for large times. As an indicator of the severity of the weakly nonlinear sea state one could use the maximum value of J. In Fig. 17 I have plotted the maximum as function of R. Also shown is the fit

$$\frac{J}{N} = \frac{R_0(1-R)}{R+R_0},\ N = \frac{\pi}{3\sqrt{3}}, \tag{A17}$$

with $R_0 = 7.44\sqrt{3}/4\pi^3$, and the fit approximates the 'exact' results reasonably well.

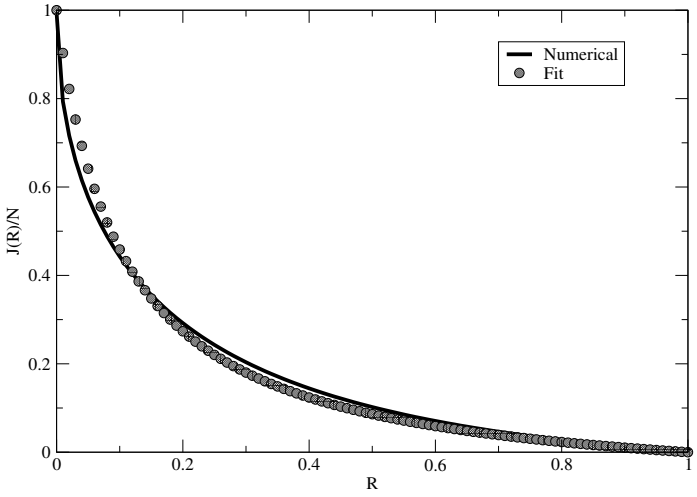

Figure 17: Maximum value of J versus R. The fit (A17) is shown as well.

A.2 Bound Waves.

The case of bound waves has been extensively discussed by Janssen (2015b). The result for general spectra will be briefly recorded, and I would also like to record the corresponding results for the case of a single wave train. It turns out, namely, that, in practice, the narrow-band limit serves as a reasonable approximation to the case of general spectra, so that these simplified results may be used in the operational implementation of the pdf of extreme events. The wave train is given by the Stokes wave solution up to third order in amplitude that is consistent with the narrow-band approximation for the general case of arbitrary spectra.

The narrow-band limit follows in a straightforward fashion from the complex function Z by using a wavenumber spectrum with a Dirac delta function, i.e. $E(\mathbf{k}) = m_0\delta(\mathbf{k}-\mathbf{k}_0)$ where m_0 is the variance of the sea surface, and $\mathbf{k}_0$ is the peak wave number. In effect, all the interaction coefficients are replaced by their value at the peak wave number. Writing

$$\mathscr{A}_{0,0} = 2\alpha, \mathscr{B}_{0,0} = 2\Delta, \mathscr{C}_{0,0,0,0} = 4\gamma, \text{ and } \mathscr{D}_{0,0,0,0} = 4\beta, \tag{A18}$$

the complex function Z becomes

$$Z = m_0 D + m_0^{1/2} A e^{i\theta} + m_0 B e^{2i\theta} + m_0^{3/2} C e^{3i\theta}, \tag{A19}$$

with $D=\Delta(a^2-\langle a^2\rangle)$, $A=a(1+\gamma\varepsilon^2 a)$, $B=\alpha a^2$, $C=\beta a^3$, and $\theta=k_0x-\omega_0t+\phi$, with ω_0 the angular peak frequency and ϕ an arbitrary phase. The coefficients α,β,γ and Δ are known functions of peak wavenumber and depth h and they read

$$\Delta=-\frac{k_0}{4}\frac{c_S^2}{c_S^2-v_g^2}\left[\frac{2(1-T_0^2)}{T_0}+\frac{1}{x}\right]+\frac{k_0^2\kappa_1}{2\omega_0\mu_1}\frac{\delta_\theta^2}{\delta_\theta^2+\alpha_\omega\delta_\omega^2},$$

$$\alpha=\frac{k_0}{4T_0^3}\left(3-T_0^2\right),\beta=\frac{3k_0^2}{64T_0^6}\left[8+\left(1-T_0^2\right)^3\right],\ \gamma=-\frac{1}{2}\alpha^2, \tag{A20}$$

where $x=k_0h$, $T_0=\tanh x$, $c_S^2=gh$, $v_g=\partial\omega/\partial k$, and $\omega_0=(gk_0T_0)^{1/2}$. The second contribution to the mean sea level term Δ is new and is calculated in Appendix B. This additional contribution illustrates nicely that the narrow-band limit of the mean sea level is not unique as it depends on the order in which the limit of vanishing width is taken.

I have used the form (A19) to calculate explicitely all the relevant statistical moments following the method in Janssen (2009, Appendix A.3). Note that in these calculations I have assumed a certain ordering of the contributions to the surface elevation. Using the significant steepness $\varepsilon=k_0m_0^{1/2}$, with typical magnitude in the range 0.01-0.05, one finds that the constant term in (A19) is of order ε^2 while the first, second and third harmonic are of order ε, ε^2 and ε^3 respectively. Calculations of the statistical moments have been performed up to lowest significant order, which means that I continue the calculation up to the first nontrivial contribution of nonlinearity.

As shown in Janssen (2014) the properties of the statistics of the bound waves are different from that of the free waves. Regarding the skewness it has been shown in Janssen (2015b) that for general spectra the following result is found:

$$\kappa_{12}=\frac{\kappa_{30}}{3},\kappa_{21}=\kappa_{03}=0, \tag{A21}$$

where κ_{30} follows from knowledge of the wave spectrum, i.e.

$$\kappa_{30}=\frac{3}{m_0^{3/2}}\int d\mathbf{k}_{1,2}E_1E_2\left(\mathscr{A}_{1,2}+\mathscr{B}_{1,2}\right), \tag{A22}$$

where the coupling coefficients are given in Janssen (2009). As a consequence one finds for the skewness factor given in Eq. (6),

$$C_3^{bound}=\frac{\kappa_{30}}{3}. \tag{A23}$$

Note that in the narrow-band limit the skewness term κ_{30} assumes the simple form

$$\kappa_{30}=6m_0^{1/2}\left(\alpha+\Delta\right), \tag{A24}$$

a result which is in agreement with Janssen (2009).

A similar analysis can be performed to obtain a general expression for the envelope kurtosis. This is a very laborious task, however, and to make sure of the result I have taken the narrow-band limit which is in perfect agreement with an expression for the envelope kurtosis for a single nonlinear wave train. Finally, the single mode expression has been validated against numerical simulation of the Stokes wave

train. Some of the details are given in the Janssen (2015b). For general spectra one finds for the envelope kurtosis κ_4 the result

$$\kappa_4 = \frac{32}{m_0^2}\int \mathrm{d}\mathbf{k}_{1,2,3}E_1E_2E_3\left\{\mathscr{A}_{1,2}\mathscr{A}_{2,3}+\mathscr{A}_{1,2}\mathscr{B}_{2,3}+\frac{1}{2}\mathscr{C}_{1+2-3,1,2,3}H_{1+2-3}\right.$$
$$\left.+\mathscr{B}_{1,3}\mathscr{B}_{3,2}\left[H_{3-2}H_{3-1}+H_{2-3}H_{1-3}\right]\right\} \tag{A25}$$

where, again, the coupling coefficients are given in Janssen (2009). Then, the bound-wave part of the kurtosis factor C_4 follows from (4), hence,

$$C_4^{bound} = \kappa_4/8. \tag{A26}$$

For a narrow-band wave train the envelope kurtosis assumes the simple form

$$\kappa_4 \quad = \quad 64m_0\left(\gamma+\alpha^2+(\alpha+\Delta)^2\right), \tag{A27}$$

and exactly the same results for the kurtosis parameters are found when one starts from the single mode representation (A19) following the method in Janssen (2009).

B Shallow water effects revisited.

B.1 Introduction.

The Benjamin-Feir instability is thought to play a key role in the formation of freak waves, resulting in a considerable amount of research on the properties of this instability. In this note I would like to concentrate on the shallow-water effects. Janssen and Onorato (2007) studied the shallow-water case and found, in agreement with Benjamin (1967), Whitham (1974), Hayes (1973), that for *one-dimensional propagation* the Benjamin-Feir instability disappears for $kh < 1.363$. This property was also shown to follow from the narrow-band version of the Zakharov equation (Zakharov, 1968) by taking appropriate limits in order to avoid apparent singularities in the nonlinear transfer coefficients.. Also, the numerical solution of the Zakharov equation showed that for $kh > 1.363$ the kurtosis was positive, while in the opposite case the sign of kurtosis changed, suggesting that there is a direct connection between the B.F. instability and the generation of freak waves.

In the present version of the ECMWF freak-wave warning system I take the BF instability into account by using the narrow-band approximation of the Zakharov equation. For example, the nonlinear transfer function becomes for 1-D propagation

$$T_{0,0,0,0}/k_0^3 = \frac{9T_0^4-10T_0^2+9}{8T_0^3}-\frac{1}{x}\left\{\frac{(2v_g-c_0/2)^2}{c_S^2-v_g^2}+1\right\}+\text{Extra.} \tag{B1}$$

where $x = k_0h$, $T_0 = \tanh x$, c_0 is the phase speed ω_0/k_0, $\omega_0 = (gk_0T_0)^{1/2}$, v_g is the group velocity $\partial\omega_0/\partial k_0$, and c_S is the wave speed in shallow water, $c_S^2 = gh$.

Numerically, it can be shown that (B1) vanishes for $k_0h = 1.363$ and that for $k_0h < 1.363$ the nonlinear transfer coefficient becomes negative suggesting that there is no freak wave formation in that case. However, this is not correct for 2-D propagation. Taking into account 2-D modulations there is instability even for $k_0h < 1.363$ as shown by Hayes (1973) and later by Davey and Stewartson (1974). Thus, the use of (B1) in estimating parameters such as the Benjamin-Feir Index is misleading, hence one needs to

consider 2-D modulations in shallow water. As explained later, it is not so straightforward to start from the Zakharov equation because the narrrow-band limit of the nonlinear transfer coefficient is awkward. I therefore used the Davey-Stewartson equations to find that there is an extra contribution to the nonlinear transfer function of the form

$$\text{Extra} = \frac{1}{4T_0}\frac{[2c_0 + v_g(1-T_0^2)]^2}{c_S^2 - v_g^2}\frac{\delta_\theta^2}{\frac{\lambda_1}{\mu_1}\delta_k^2 + \delta_\theta^2}. \tag{B2}$$

which is always positive, therefore this tends to enhance the nonlinear transfer. Here, δ_θ and δ_k are the relative spectral widths in $\theta-$space and $k-$space, respectively. Note that the dependence on the width of spectrum is rather peculiar: the limiting value depends on the order in which the limits of δ_θ and δ_k are taken. Therefore, in the presence of the wave-induced current induced by modulations that have a transverse wavenumber dependence the narrow-band limit is not unique. This is a problematic feature when one is interested in the narrow-band limit on the nonlinear transfer coefficient, but this problem can be resolved by explicitely taking into account the dependence on the modulation wavenumbers in the along and the cross direction with respect the propagation direction.

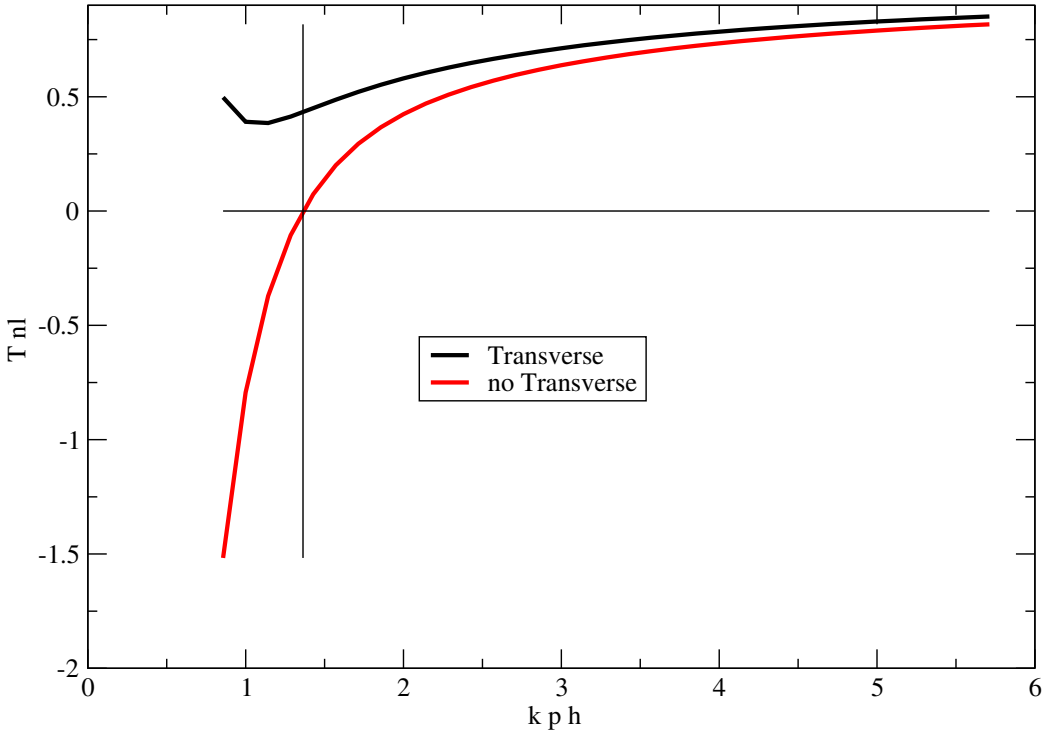

Figure 18: Nonlinear transfer coefficient with and without transverse modulations as a function of dimensionless depth k_0h.

As an illustration of the transverse effect I have plotted in Fig. 18 the nonlinear transfer coefficient $T_{0,0,0,0}$ normalised with the factor k_0^3 as a function of dimensionless depth k_0h for two cases. The first case has equal width in frequency and direction, while the second case is for vanishing directional width. The last case has a vanishing nonlinear transfer for $k_0h = 1.363$ as is indicated by the cross in the figure. It is clear that directional effects in shallow water play an important role, resulting in modulational instability far beyond the one-dimensional threshold value of 1.363.

B.2 Derivation of narrow-band nonlinear transfer coefficient.

My starting point is the Davey-Stewartson equations. There are several forms of this equation available. I will take the set which is based on the action variable. Introduce the action variable $A(\mathbf{k})$ defined in such a way that the surface elevation η reads

$$\eta = \int \mathrm{d}\mathbf{k} \left(\frac{\omega}{2g}\right)^{1/2} (A(\mathbf{k}) + A^*(-\mathbf{k})) \exp(i\mathbf{k}\cdot\mathbf{x}). \tag{B3}$$

For a single mode $A(\mathbf{k}) = A\delta(\mathbf{k}-\mathbf{k}_0)$, assuming without loss of generality that the carrier wave with wavenumber k_0 propagates in the x-direction, one then finds

$$\eta = \left(\frac{\omega_0}{2g}\right)^{1/2} \left(Ae^{ik_0x} + A^*e^{-ik_0x}\right). \tag{B4}$$

The Davey-Stewartson equations for the envelope A and wave-induced current Q, caused by transverse modulations, then become

$$i\frac{\partial A}{\partial \tau} + \lambda\frac{\partial^2 A}{\partial x^2} + \mu\frac{\partial^2 A}{\partial y^2} = \nu|A|^2A + \nu_1 QA$$

$$\lambda_1\frac{\partial^2 Q}{\partial x^2} + \mu_1\frac{\partial^2 Q}{\partial y^2} = \kappa_1\frac{\partial^2|A|^2}{\partial y^2} \tag{B5}$$

where

$$\lambda = \frac{1}{2}\omega''(k_0),\ \mu = v_g/2k_0,\ c_0 = \omega_0/k_0,$$

$$\nu = k_0^3\left[\frac{9T_0^4 - 10T_0^2 + 9}{8T_0^3} - \frac{1}{x}\left\{\frac{(2v_g - c_0/2)^2}{c_S^2 - v_g^2} + 1\right\}\right],$$

$$\nu_1 = \frac{k_0^4}{2\omega_0 v_g}\left\{2c_0 + v_g(1-T_0^2)\right\},\ \lambda_1 = c_S^2 - v_g^2,\ \mu_1 = c_S^2,$$

$$\kappa_1 = \frac{1}{2}\frac{c_0}{T_0}c_S^2 v_g\frac{2c_0 + v_g(1-T_0^2)}{c_S^2 - v_g^2}. \tag{B6}$$

The basic solution of Eq. (B5) is the uniform Stokes solution

$$A = a_0 e^{[-i(\nu a_0^2 + \nu_1 Q_0)\tau]},\ Q = Q_0 = \text{constant}, \tag{B7}$$

and to test the stability of this traveling wave one introduces modulations according to

$$A = a_0\{1 + \varepsilon a(\mathbf{x},t)\}e^{[-i(\nu a_0^2 + \nu_1 Q_0)\tau]},$$

$$Q = Q_0(1 + \varepsilon q(\mathbf{x},t)) \tag{B8}$$

with $a = a_+E + a_-E^{-1}$, $q = q_+E + q_-e^{-1}$, where $E = \exp i(lx + my - \Omega\tau)$.

Linearizing Eqns. (B5) while using the form (B8) the resulting dispersion relation for Ω as function of wavenumber l and m becomes

$$\Omega^2 = \left(\lambda l^2 + \mu m^2\right)\left[2\tilde{\nu}a_0^2 + (\lambda l^2 + \mu m^2)\right] \tag{B9}$$

where

$$\tilde{\nu} = \nu + \nu_1\kappa_1 m^2/(\lambda_1 l^2 + \mu_1 m^2).$$

From (B9) Hayes (1973) and Davey and Stewartson (1974) showed that the wave train is unstable if

$$\tilde{\nu}(\lambda l^2 + \mu m^2) < 0. \tag{B10}$$

Note that λ is always negative, μ is positive and ν changes from negative to positive as k_0h increase beyond $k_0h = 1.363$ (Hasimoto and Ono, 1972).

Hayes (1973) has shown that it is always possible to choose l and m in such a way that the instability criterion (B10) is satisfied, but instability is practically non-existent for shallow water waves in the range $0 \leq k_0h \leq 0.5$.

The severity of the sea state is usually estimated by means of the Benjamin-Feir Index which measures the balance of nonlinearity and dispersion. Here, the measure of importance of nonlinearity is given by the coefficient $\tilde{\nu}$ in the dispersion relation (B9),

$$\tilde{\nu} = \nu + \nu_1\kappa_1 m^2/(\lambda_1 l^2 + \mu_1 m^2).$$

Note that in the one-dimensional shallow water case one finds $\tilde{\nu} = \nu$ as m then vanishes. This is the expression that has been used so far in the ECMWF freak wave warning system. The 2-D effect is entirely caused by the term $\nu_1\kappa_1 m^2/(\lambda_1 l^2 + \mu_1 m^2)$. Clearly, the narrow-band limit of this term is not unique as it depends on the order in which the limits $l \to 0$ and $m \to 0$ are taken. Therefore, in this extra contribution spectral width needs to be taken into account explicitely.

In the next step we need to estimate the size of the modulation wavenumbers l and m. I will do this in terms of the frequency and directional width σ_ω and σ_θ. Writing the original wave numbers k_x and k_y in terms of the polar coordinates k and θ the modulation wave numbers l and m become

$$l = k_x - k_0 = k\cos\theta - k_0,\ m = k_y = k\sin\theta,$$

and expanding around the values $k = k_0$ and $\theta = 0$ one finds in lowest order

$$\delta l = \delta k,\ \delta m = k_0\delta\theta,$$

therefore

$$\langle\delta l^2\rangle^{1/2} = \sigma_k,\ \langle\delta m^2\rangle^{1/2} = k_0\delta_\theta.$$

Finally, introducing the relative frequency width δ_ω using the relation $\delta_\omega = \sigma_\omega/\omega_0 = v_g/c_0 \times \sigma_k/k_0$ the extra term E becomes

$$E = \frac{\kappa_1\nu_1}{\mu_1}\frac{\delta_\theta^2}{\delta_\theta^2 + \alpha_\omega\delta_\omega^2}$$

with $\alpha_\omega = \lambda_1 c_0^2/\mu_1 v_g^2$. This parametrization of the effects of 2D modulations has the desirable property that for a narrow directional distribution with $\delta_\theta \to 0$ the extra contribution vanishes. The front factor

$\kappa_1\nu_1/\mu_1$ and the factor α_ω can be written more explicitely using the expressions for κ_1, ν_1, μ_1 and λ_1. Then α_ω becomes

$$\alpha_\omega = \frac{c_0^2}{v_g^2}\left(1 - \frac{v_g^2}{c_S^2}\right) \tag{B11}$$

and the extra term becomes explicitely

$$E = \frac{k_0^3}{4T_0}\frac{\left[2c_0 + v_g(1-T_0^2)\right]^2}{c_S^2 - v_g^2}\frac{\delta_\theta^2}{\delta_\theta^2 + \alpha_\omega\delta_\omega^2} \tag{B12}$$

In principle, the extra term depends on the ratio $\delta_\theta/\delta_\omega$ which can be eliminated in favour of the ratio R defined in (A14).

Note that the additional contribution to the nonlinear transfer coefficient is associated with a finite value of the wave-induced current caused by the two-dimensional modulations, hence a finite value of Q. In terms of the amplitude a of the surface elevation (here action variable $A = (g/2\omega_0)^{1/2}a$) the above result implies that

$$Q = \frac{\kappa_1 g}{2\omega_0\mu_1}\frac{\delta_\theta^2}{\delta_\theta^2 + \alpha_\omega\delta_\omega^2}|a|^2 \tag{B13}$$

and the additional contribution to the wave-induced current is given by k^2Q/v_g (see Eq. (B19)). This will give rise to an additional contribution to the mean sea level. Using Eq. (2.13c) of Davey and Stewartson (1974) one then finds for the mean sea level η_{20} the explicit expression

$$\eta_{20} = -\frac{k_0 c_S^2}{4(c_S^2 - v_g^2)}\left(\frac{2(1-T_0^2)}{T_0} + \frac{1}{x}\right)|a|^2 + \frac{k_0^2\kappa_1}{2\omega_0\mu_1}\frac{\delta_\theta^2}{\delta_\theta^2 + \alpha_\omega\delta_\omega^2}|a|^2 \tag{B14}$$

Clearly, also the narrow-band limit of the mean sea level is not unique and therefore one has to take explicit account of the spectral widths.

In order to illustrate the importance of the wave-induced mean sea level caused by the directional width of the wave spectrum I have compared in Fig. 19 mean sea levels with (black circles) and without (red circles) the two-dimensional contribution against exact computations of the wave-induced sea level. These exact computations do not include the two-dimensional contribution as the interaction coefficients have been determined by taking the limit for a one-dimensional wave spectrum. Therefore, the model calculations without the transverse effect are in good agreement with the exact result. It is clear, however, that the transverse contribution reduces the size of the wave-induced mean sea level.

Recently, there has been a considerable in interest in the role of the wave-induced mean sea level in the severity of the sea state of the Draupner case. In the one-dimensional case there is a set down due to the presence of the weakly nonlinear waves and in practice this will give rise to reduced levels of skewness and kurtosis (see (A24) and (A27)). However, as is also evident from Eq. (B14), two-dimensional effects may reduce the size of the set down and may, in principle, even give rise to a wave-induced set up. Using the simulated spectra from the WAM model for the Draupner case, the exact computations always give rise to a set down, however, as is evident from Fig. (19). In order to explore the possibility of a wave-induced set up further, I have plotted in Fig 20 the dimensionless mean sea level $\langle\eta_{20}\rangle/(2\varepsilon m_0^{1/2})$ as function of dimensionless depth for three values of the ratio $\delta_\theta/\delta_\omega$, namely 0, 1 and ∞. Although for broader directional spectra the wave-induced mean sea level almost vanishes, there is hardly no indication of a wave-induced set up.

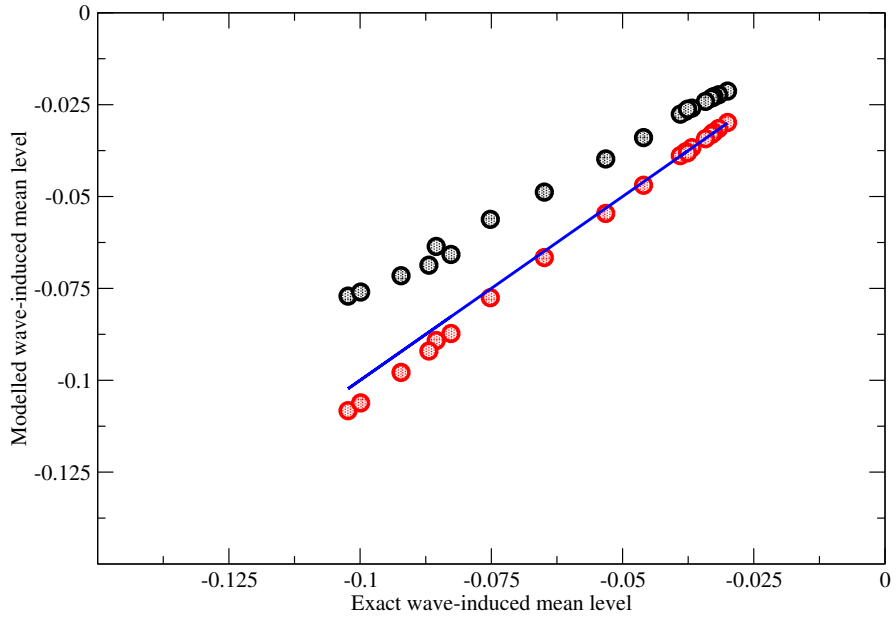

Figure 19: Comparison of wave-induced mean sea level with (black circles) and without transverse effect (red circles) against exact computations for the Draupner case, showing that the transverse effect is relevant. The blue line is the line of perfect agreement.

B.3 Rederive Davey-Stewartson Equations.

While trying to derive the effect of 2-D modulations on the nonlinear transfer function from the Davey-Stewartson equations, it was realized that one of its coefficients was not dimensionally correct, namely ν_1. Furthermore, checking the derivation by the authors a magical factor (2.23) was introduced without mentioning the physical interpretation of the factor Q. Let us redo a bit of their derivation, my version of it will give a dimensionally correct coefficient ν_1, while it is quite clear that Q turns out to be connected with the extra flow induced by the 2-dimensional modulation. In order to understand this section the availability of Davey and Stewartson (1974) will be essential, while it is emphasized that the original D&S equatuations are for the envelope amplitude of the potential and not of the action variable.

Let us start from their Equations (2.14) and (2.15). They read, with ϕ_{01} the amplitude of the mean flow potential,

$$(c_S^2 - v_g^2)\frac{\partial^2\phi_{01}}{\partial\xi^2} + c_S^2\frac{\partial^2\phi_{01}}{\partial\eta^2} = -k^2\left\{2c_0 + v_g(1-T_0^2)\right\}\frac{\partial|A|^2}{\partial\xi} \tag{B15}$$

while, with A the amplitude of the potential oscillation,

$$2i\omega\frac{\partial A}{\partial\tau} - \left\{v_g^2 - c_S^2(1-T_0^2)(1-khT_0)\right\}\frac{\partial^2 A}{\partial\xi^2} + c_0 v_g\frac{\partial^2 A}{\partial\eta^2} =$$
$$\frac{1}{2}k^4\left\{T_0^{-2} - 12 + 13T_0^2 - 2T_0^4\right\}|A|^2A + k^2\left\{2c_0 + v_g(1-T_0^2)\right\}A\frac{\partial\phi_{01}}{\partial\xi}. \tag{B16}$$

Here, $\tau = \varepsilon^2 t, \xi = \varepsilon(x - v_g t), \eta = \varepsilon y$, and ε is assumed to be small.

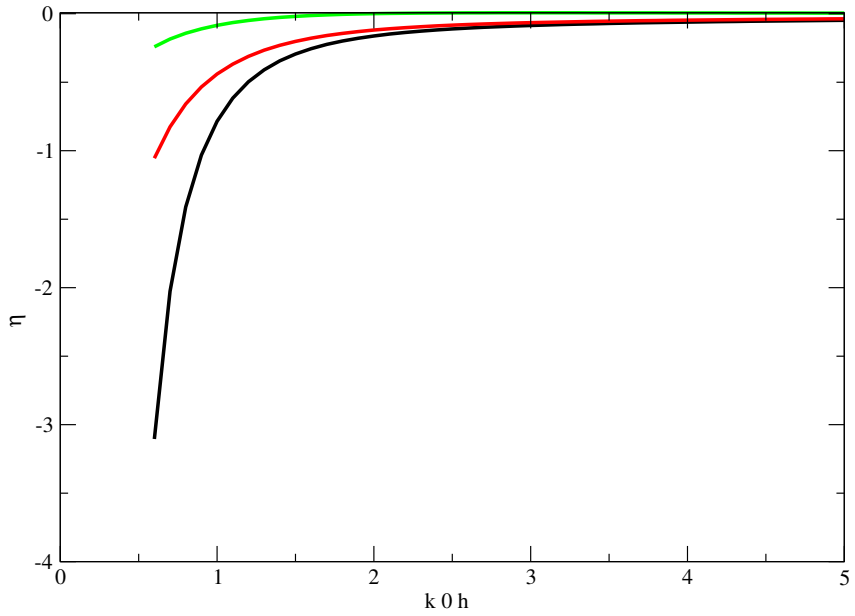

Figure 20: Comparison of wave-induced mean sea level $\langle \eta_{20} \rangle / (2\varepsilon m_0^{1/2})$ as function of dimensionless depth $k_o h$ for different values of the ratio $\delta_\theta / \delta_\omega$, namely 0 (black line), 1 (red line) and ∞ (green line).

The 1-D problem.

Consider the 1-D problem first, so disregard derivatives with respect to η. The equation for the mean potential ϕ_{01} may then be integrated once to obtain

$$\frac{\partial \phi_{01}}{\partial \xi} = -k^2/\lambda_1 \left\{ 2c_0 + v_g(1 - T_0^2) \right\} |A|^2 \tag{B17}$$

where $\lambda_1 = c_S^2 - v_g^2$. Then, substitute (B17) in (B16) to obtain

$$i\frac{\partial A}{\partial \tau} + \lambda \frac{\partial^2 A}{\partial \xi^2} = \nu |A|^2 A \tag{B18}$$

with

$$\nu = 2\frac{k^4 T_0}{\omega} \left[\frac{9 - 10T_0^2 + 9T_0^4}{8T_0^3} - \frac{1}{x} \left\{ \frac{(2v_g - c_0/2)^2}{c_S^2 - v_g^2} + 1 \right\} \right]. \tag{B19}$$

Note that after some extensive algebra the second term in Davey and Stewartson (1974) may be written in the form given in (B19) which agrees with the results from Whitham (1974).

The 2-D problem.

Eq. (B17) gives the 'equilibrium' flow for a 1-dimensional modulation. Clearly, in 2-D there will be an additional contribution to the flow. Thus we introduce the factor Q according to

$$\frac{\partial \phi_{01}}{\partial \xi} = k^2 Q / v_g - k^2/\lambda_1 \left\{ 2c_0 + v_g(1 - T_0^2) \right\} |A|^2 \tag{B20}$$

where the last term corresponds to the right-hand side of (B17). Now substitute (B20) in (B15) to obtain an equation for transverse contribution to the flow, Q,

$$\lambda_1 \frac{\partial^2 Q}{\partial \xi^2} + c_S^2 \frac{\partial^2 Q}{\partial \eta^2} = \kappa_1 \frac{\partial^2 |A|^2}{\partial \eta^2} \tag{B21}$$

where $\lambda_1 = c_S^2 - v_g^2$ while

$$\kappa_1 = \frac{v_g c_S^2}{c_S^2 - v_g^2} \left\{ 2c_0 + v_g \left(1 - T_0^2\right) \right\} \tag{B22}$$

which agrees with Davey and Stewartson (1974) (Note that $c_S^2 = gh$).

Finally, substituting (B20) in (B16) gives

$$i \frac{\partial A}{\partial \tau} + \lambda \frac{\partial^2 A}{\partial \xi^2} + \mu \frac{\partial^2 A}{\partial \eta^2} = \nu |A|^2 A + \nu_1 Q A, \tag{B23}$$

where $\lambda = \omega_0''/2, \mu = v_g/2k$, ν is given in Eq. (B19) and, finally,

$$\nu_1 = \frac{k^4}{2\omega v_g} \left\{ 2c_0 + v_g \left(1 - T_0^2\right) \right\} \tag{B24}$$

which has, compared to Davey and Stewartson (1974), an additional factor of $1/2\omega$.

References

Adler, R.J., 1981. *The Geometry of Random Fields*, John Wiley, 275 pp.

Benetazzo, A., F. Barbariol, F. Bergamasco, A. Torsello, S. Carniel, and M. Sclavo, 2015. Observation of Extreme Sea Waves in a Space-Time Ensemble. *J. Phys. Oceanogr.* **45**, 2261-2275.

Baxevani, A. and I. Rychlik, 2006. Maxima for Gaussian Seas. *Ocean Eng.* **33**, 895-911

Benjamin, T.B., 1967. Instability of periodic wavetrains in nonlinear dispersive systems. *Proc. Roy. Soc. A* **299**, 59-75.

Benjamin, T.B., and J.E. Feir, 1967: The desintegration of wavetrains on deep water. Part 1. Theory. *J. Fluid Mech.* **27**, 417-430.

Burgers, G., F. Koek, H. de Vries and M. Stam, 2008. Searching for factors that limit observed extreme maximum wave height distributions in the North Sea. *Extreme Ocean Waves*, E. Pelinovsky and C. Kharif (eds), Springer Science+Business Media B.V., pp. 127-138.

Cavaleri, L., F. Barbariol, A. Benetazzo, L. Bertotti, J.-R. Bidlot, Peter A.E.M. Janssen and Nils Wedi, 2016. The Draupner wave: a fresh look and the emerging view.

Davey, A. & K. Stewartson, 1974. On three-dimensional packets of surface waves. *Proc. R. Soc. Lond.***A 338**, 101-110.

Dean, R.G., 1990. Freak waves: A possible explanation. In A. Torum & O.T. Gudmestad (Eds.), *Water Wave Kinematics* (pp. 609-612), Kluwer.

Draper, L., 1965. 'Freak' ocean waves. *Marine Observer* **35**, 193-195.

Elgar, S., R.T. Guza and R.J. Seymour, 1984. Groups of Waves in Shallow Water. *J. Geophys. Res.* 89, 3623-3634.

Fedele F., 2012. Space-Time Extremes in Short-Crested Storm Seas. *J. Phys. Oceanogr.* **42**, 1601-1615.

Fedele F., 2015. On the kurtosis of deep-water gravity waves. *J. Fluid Mech.* **782**, 25-36.

Goda, Y., 2000. *Random seas and Design of Maritime Structures*. 2nd ed. World Scientific, 464 pp.
Hayes, W.D., 1973. Group velocity and nonlinear dispersive wave propagation. *Proc. R. Soc. Lond.* **A 332**, 199-221.

Hasimoto, H. & H. Ono, 1972. *J. Phys. Soc. Japan*, **33**, 805.

Hayes, W.D., 1973. Group velocity and nonlinear dispersive wave propagation. *Proc. R. Soc. Lond.* **A 332**, 199-221.

Janssen, Peter A.E.M., 2003. Nonlinear Four-Wave Interactions and Freak Waves. *J. Phys. Oceanogr.* **33**, 863-884.

Janssen, Peter A.E.M., 2009. On some consequences of the canonical transformation in the Hamiltonian theory of water waves, *J. Fluid Mech.* **637**, 1-44.

Janssen, Peter A.E.M., 2014. On a random time series analysis valid for arbitrary spectral shape, *J. Fluid Mech.* **759**, 236-256.

Janssen, Peter A.E.M., 2015a, Notes on the maximum wave height distribution. ECMWF Technical Memorandum 755.

Janssen, Peter A.E.M., 2015b, How rare is the Draupner wave event? ECMWF Technical Memorandum 775.

Janssen, Peter A.E.M., 2017, Random note on statistics of a nonlinear system, ECMWF.

Janssen Peter A.E.M and Miguel Onorato, 2007. The intermediate water depth limit of the Zakharov Equation and consequences for wave prediction, *J. Phys. Oceanogr.* **37**, 2389-2400.

Janssen, Peter A.E.M., and Jean-R. Bidlot, 2009. On the extension of the freak wave warning system and its verification. ECMWF Technical Memorandum 588.

Longuet-Higgins, M.S., 1983. On the joint distribution of wave periods and amplitudes in a random wave field. *Proc. Roy. Soc. London* **A389**, 241-258.

Magnusson, A.K. and M.A. Donelan, 2013. The Andrea wave Characteristics of a Measured North Sea Rogue Wave. Transactions of the ASME Journal of Offshore Mechanics and Arctic Engineering, **135**, 031108-3.

Montina, A., U. Bortolozzo, S. Residori, and F.T. Arecchi, 2009. Non-Gaussian Statistics and Extreme Waves in a Nonlinear Optical Cavity, PRL **103**, 173901.

Mori N. and P.A.E.M. Janssen, 2006. On kurtosis and occurrence probability of freak waves. *J. Phys. Oceanogr.* **36**, 1471-1483.

Naess, A., 1982. Extreme value estimates based on the envelope concept. *Applied Ocean research*, **1982**, 181-187.

Stefania Residori, 2015. Private communication and presentation at Cargèse summerschool on Rogue Waves.

Walczak, Pierre, Stéphane Randoux, and Pierre Suret, 2015. Optical Rogue Waves in integrable turbulence. PRL **114**, 143903.

Whitham, G.B., 1974. *Linear and Nonlinear Waves*. Wiley, New York.

Worsley, K.J., 1996. The geometry of random images. *Chance*, **9**, 27-40.

Zakharov, V.E., 1968. Stability of periodic waves of finite amplitude on the surface of a deep fluid. *J. Appl. Mech. Techn. Phys.* **9**, 190-194.